

1 **Carbon emission and export from Ket River, western Siberia**

2  
3 **Artem G. Lim<sup>1</sup>, Ivan V. Krickov<sup>1</sup>, Sergey N. Vorobyev<sup>1</sup>,**

4 **Mikhail A. Korets<sup>2</sup>, Sergey Kopysov<sup>1</sup>,**

5 **Liudmila S. Shirokova<sup>3</sup>, Jan Karlsson<sup>4</sup>, and Oleg S. Pokrovsky<sup>5\*</sup>**

6  
7 *<sup>1</sup>BIO-GEO-CLIM Laboratory, Tomsk State University, Tomsk, Russia*

8 *<sup>2</sup>V.N. Sukachev Institute of Forest of the Siberian Branch of Russian Academy of Sciences – separated*  
9 *department of the KSC SB RAS, Krasnoyarsk, 660036, Russia*

10 *<sup>3</sup>N. Laverov Federal Center for Integrated Arctic Research, Russian Academy of Sciences, Arkhangelsk,*  
11 *Russia*

12 *<sup>4</sup>Climate Impacts Research Centre (CIRC), Department of Ecology and Environmental Science, Umeå*  
13 *University, Linnaeus väg 6, 901 87 Umeå, Sweden.*

14 *<sup>5</sup>Geosciences and Environment Toulouse, UMR 5563 CNRS, 14 Avenue Edouard Belin 31400 Toulouse,*  
15 *France*

16  
17 Key words: CO<sub>2</sub>, C, emission, boreal, river, export, landscape, Siberia

18  
19 \* email: oleg.pokrovsky@get.omp.eu

18

19

20

21

22

23

24

25

26

27

28

29

30

31

32

33           **Abstract**

34           Despite recent progress in the understanding of the carbon (C) cycle of Siberian permafrost-affected  
35 rivers, spatial and seasonal dynamics of C export and emission from medium-size rivers (50,000 - 300,000  
36 km<sup>2</sup> watershed area) remain poorly known. Here we studied one of the largest tributaries of the Ob River, the  
37 Ket River (watershed = 94,000 km<sup>2</sup>) which drains through pristine taiga forest of the boreal zone in western  
38 Siberian Lowland (WSL). We combined continuous and discrete measurements of carbon dioxide (CO<sub>2</sub>)  
39 concentration using submersible CO<sub>2</sub> sensor and floating chamber flux (FCO<sub>2</sub>), with methane (CH<sub>4</sub>), organic  
40 and inorganic C (DOC and DIC, respectively), particulate organic C and total bacterial concentrations over a  
41 800-km transect of the Ket River main stem and its 26 tributaries during spring flood (May 2019) and 12  
42 tributaries during summer baseflow (end of August – beginning of September 2019). The partial pressure of  
43 CO<sub>2</sub> (pCO<sub>2</sub>) was lower and less variable in the main stem (2000 to 2500 μatm) compared to that in tributaries  
44 (2000 to 5000 μatm). In the tributaries, the pCO<sub>2</sub> was 40 % higher during baseflow compared to spring flood,  
45 whereas in the main stem, it did not vary significantly across the seasons. The methane concentration in the  
46 main stem and tributaries was a factor of 300 to 1900 (flood period) and 100 to 150 times lower than that of  
47 CO<sub>2</sub>, and ranged from 0.05 to 2.0 μmol L<sup>-1</sup>. The FCO<sub>2</sub> ranged from 0.4 to 2.4 g C m<sup>-2</sup> d<sup>-1</sup> in the main channel  
48 and from 0.5 to 5.0 g C m<sup>-2</sup> d<sup>-1</sup> in the tributaries, being the highest during August in tributaries and weakly  
49 dependent on season in the main channel. During summer baseflow, the **DOC** aromaticity, bacterial number,  
50 and needleleaf forest coverage of the watershed positively affected CO<sub>2</sub> concentrations and fluxes. We  
51 hypothesize that relatively low spatial and seasonal variability in FCO<sub>2</sub> of the Ket River is due to flat  
52 homogeneous landscape (bogs and taiga forest) that results in long water residence times and stable input of  
53 allochthonous DOM, which dominate the FCO<sub>2</sub>. The open water period (May to October) C emission from  
54 the fluvial network (main stem and tributaries) of the Ket River was estimated to 127±11 Gg C y<sup>-1</sup> which is  
55 lower than the downstream dissolved and particulate C export during the same period. The estimated fluvial  
56 C emissions are highly conservative and contain uncertainties, linked to ignoring hot spots and hot moments  
57 of emissions, notably in the floodplain zone. This stresses the need of improving temporal resolution of FCO<sub>2</sub>  
58 and water coverage across seasons and emphasizes the important role of WSL rivers for release of CO<sub>2</sub> to the  
59 atmosphere.

## 60 **Introduction**

61 Assessment of greenhouse gas (GHG) emission from rivers is crucially important for understanding  
62 the C cycle under various climate change scenarios (Campeau and del Giorgio, 2014; Chadburn et al., 2017;  
63 Tranvik et al., 2018; Vonk et al., 2019; Vachon et al., 2020). Rivers receive terrestrial C and process and emit  
64 a significant share of this C during transit to the sea (Liu et al., 2022). Quantifications of riverine C emissions  
65 are sufficiently robust for relatively well studied regions of the world such as the European and N American  
66 boreal zone (Dawson et al., 2004; Dinsmore et al., 2013; Wallin et al., 2013; Leith et al., 2015; Zolkos et al.,  
67 2019; Hutchins et al., 2020), or Arctic and subarctic rivers of Alaska (Striegl et al., 2012; Crawford et al.,  
68 2013; Stackpoole et al., 2017), although subjected to great uncertainty. Despite significant progress in  
69 assessing riverine pCO<sub>2</sub> in previously under-represented or ignored regions such as lotic systems of Asia (Ran  
70 et al., 2015, 2017; Varol and Li, 2017) or South America (Almeida et al., 2017), these studies generally use  
71 a combination of pH and alkalinity (DIC) to calculate the pCO<sub>2</sub> instead of direct in-situ measurements, alike  
72 the studies of global emissions (Raymond et al., 2013; Lauerwald et al., 2015). At the same time, there is a  
73 growing number of studies reporting directly measured riverine pCO<sub>2</sub> – either discretely (Alin et al. 2011;  
74 Borges et al., 2015; Amaral et al. 2018; 2022; Leng et al. 2022), continuously at fixed sites (Crawford et al.  
75 2016a, Schneider et al. 2020; Gómez-Gener et al. 2021a), or along the river flow (Abril et al. 2014; Crawford  
76 et al. 2016b; 2017; Borges et al. 2019). However, these studies are limited to tropical and temperate zones of  
77 the world, and boreal regions of Western Europe and Northern America, and thus, further continuous and  
78 discrete measurements of CO<sub>2</sub> concentration and fluxes in rivers from under-represented regions such as  
79 Northern Eurasia, and in particular, Siberia, are needed. The on-going interest to Siberia comes from the fact  
80 that this region hosts large C stocks in soils and wetlands intersected by extensive river networks that deliver  
81 majority of water and C to the Arctic Ocean (Feng et al., 2013).

82 A few works on Siberian fluvial systems dealt with small (Castro-Morales et al., 2022) and large  
83 (Denfeld et al., 2013; Vorobyev et al., 2021) rivers, but these were performed in Eastern Siberia, under  
84 continuous permafrost zone. More progress has been achieved in quantification of downstream carbon export  
85 by permafrost-affected Great Arctic Rivers of Siberia (Lobbés et al., 2000; Raymond et al., 2007; Cooper et  
86 al., 2008; Semiletov et al., 2011; Feng et al., 2013; Griffin et al., 2018; Wild et al., 2019). However, spatial

87 and seasonal features of C emission from tributaries of large Siberian rivers are still remain poorly known.  
88 Existing data on western Siberia (Serikova et al., 2018; Karlsson et al., 2021) suggest that C (predominantly  
89 as CO<sub>2</sub>) emissions from rivers can vary largely over space and time. Such high variations do not allow reliable  
90 quantitative assessment of C emission and integrating these values into regional and global C models.

91 In order to better understand and constrain the magnitude of C emission from Siberian rivers, we  
92 studied the Ket River (watershed 94,000 km<sup>2</sup>), a typical tributary of the Ob River in western Siberia. The Ob  
93 river is the largest (in terms of watershed area) Siberian river and drains large pristine territories of taiga forest  
94 and bogs. The catchment of Ob includes extensive regions of permafrost but a major part of it (> 80 %) is  
95 situated in the permafrost-free zone of which very few data exist on riverine C emissions (Karlsson et al.,  
96 2021). The Ket river drains through dense southern taiga forest and abundant wetlands with almost no human  
97 activity, thus serving a representative system for understanding C cycling in permafrost-free Siberian rivers.  
98 We followed, via a boat routing over the main stem and main tributaries of the river, the in-situ CO<sub>2</sub>  
99 concentrations combined with discrete sampling for dissolved CH<sub>4</sub>, DOC, DIC, total bacterial number and  
100 particulate organic matter. These measurements were complemented with regular floating chamber  
101 measurements of CO<sub>2</sub> emission fluxes. We performed these observations during two main open water seasons  
102 of the year - the peak of the spring flood and the end of the summer baseflow. Our first objective was to  
103 quantify the difference in C concentration and emission during two seasons for the main stem and the  
104 tributaries and to relate these differences to main physico-chemical parameters of the water column and  
105 physio-geographical parameters (land cover) of the river watersheds. Our second objective was to obtain total  
106 C emission flux from the river watershed area and compare it to downstream export yield of dissolved and  
107 particulate carbon.

108

## 109 **2. Study Site, Materials and Methods**

### 110 *2.1. Ket River and its tributaries*

111 The Ket River main stem and its 26 tributaries sampled in this study include watersheds of distinct  
112 sizes (catchment area ranged from 94,000 km<sup>2</sup> at the Ket's mouth to 20 km<sup>2</sup> of smallest tributary), but rather  
113 similar lithology, climate and vegetation (**Fig. 1, Table S1**). The Strahler's order of sampled rivers and stream

114 ranges from 9 for Ket at its mouth to 2 for the smallest stream. The poorly accessible Ket River basin is fully  
115 pristine (50 % forest, 40 % wetlands), and has almost no agricultural and forestry activity. The watershed of  
116 Ket has very low population density (0.27 person km<sup>-2</sup>) and lacks road infrastructure due to absence of oil  
117 and gas development and production. In this regard, this river can serve as a model for medium size bog-  
118 forest rivers of the western Siberia Lowland and results obtained from this watershed can be extrapolated to  
119 much larger territory, comprising about 1 million km<sup>2</sup> of permafrost-free taiga forest and bog regions of the  
120 southern part of WSL.

121 The mean annual air temperatures (MAAT) is  $-0.7 \pm 0.1$  °C and the mean annual precipitation is  $520$   
122  $\pm 20$  mm y<sup>-1</sup> in the central part of the basin. The lithology of this part of western Siberian lowland is dominated  
123 by Pleistocene silts and sands with carbonate concretions overlaid by quaternary deposits (loesses, fluvial,  
124 glacial and lacustrine deposits). The dominant soils are podzols in forest areas and histosols in peat bog  
125 regions. Further description of climate, lithology and landscape features of the territory is provided in former  
126 studies (Frey and Smith, 2007; Pokrovsky et al., 2015).

127 The peak of annual discharge in 2019 occurred in the end of May; in August, the discharge was 3 to  
128 5 times smaller (**Fig. 1**). Note that low runoff, lack of relief and highly homogenous landscape coverage of  
129 the permafrost-free zone of western Siberia in general and of the Ket River basin in particular provide quite  
130 smooth hydrographs of the rivers. In this regard, the spring flood period is extended over 2 months, from the  
131 beginning of May to middle of July, whereas summer baseflow includes second half of July, August and  
132 September. As a result, similar to previous study of rivers along a 2500 km transect of the WSL territory, the  
133 timing of the two sampling campaigns covered approximately 80% of the annual water discharge in the basins  
134 (Serikova et al., 2018). From May 18 to May 28, 2019, and from August 30 to September 2, 2019, we started  
135 the boat trip in the middle course of the Ket River (Beliy Yar), and moved, first, 475 km upstream the Ket  
136 river till its most headwaters, and then moved 834 km downstream till the river mouth, with an average speed  
137 of 20 km h<sup>-1</sup>. During summer baseflow, the 4-days trip was shortened by 200 km due to too low water level  
138 in the upper reaches of the main stem and some small tributaries. We stopped each 30-50 km along the Ket  
139 River and sampled for major hydrochemical parameters, GHG, river suspended matter and total bacterial  
140 number of the main stem. We also moved several km upstream of selected tributaries to record CO<sub>2</sub>

141 concentrations for at least 1 h and to sample for river hydrochemistry. At several occasions during spring  
142 flood, we monitored CO<sub>2</sub> concentration and performed chamber measurements in the main stem and  
143 tributaries during both day and night time period.

144

## 145 2.2. CO<sub>2</sub> and CH<sub>4</sub> concentrations and CO<sub>2</sub> fluxes by floating chambers

146 Surface water CO<sub>2</sub> concentration was measured continuously, *in-situ* by deploying a portable infrared  
147 gas analyzer (IRGA, GMT222 CARBOCAP® probe, Vaisala®; accuracy ± 1.5%) of two ranges (2 000 and  
148 10 000 ppm) as described in previous work of our group on the Lena River (Vorobyev et al., 2021). Sensor  
149 preparation was conducted in the lab following the method described by Johnson et al. (2009). The  
150 measurement unit (MI70, Vaisala®; accuracy ± 0.2%) was connected to the sensor allowing instantaneous  
151 readings of *p*CO<sub>2</sub>. The sensors were calibrated in the lab against standard gas mixtures (0, 800, 3 000, 8 000  
152 ppm; linear regression with R<sup>2</sup> > 0.99) before and after the field campaign. The sensors' drift was 0.03-0.06%  
153 per day and overall error was 4-8% (relative standard deviation, RSD). Following calibration, post-  
154 measurement correction of the sensor output induced by changes in water temperature and barometric  
155 pressure was done by applying empirically derived coefficients following Johnson et al. (2009). These  
156 corrections never exceeded 5% of the measured values. During the cruise, we routinely measured atmospheric  
157 CO<sub>2</sub> with the probe as a check for its good functioning. Furthermore, we tested two different sensors in several  
158 sites of the river transect: a main probe used for continuous measurements and another probe used as a control  
159 and never employed for continuous measurements. We did not find any sizable (>10%) difference in  
160 measured CO<sub>2</sub> concentration between these two probes.

161 The probe was enclosed within a waterproof and gas-permeable membrane. For this, we used a  
162 protective expanded polytetrafluoroethylene (PTFE) sleeve that is highly permeable to CO<sub>2</sub> but impermeable  
163 to water (Johnson et al., 2009). The sensor was placed into a tube which was submerged 0.5 m below the  
164 water surface. A Campbell logger was connected to the system allowing continuous recording of the CO<sub>2</sub>  
165 concentration, water temperature and pressure every minute. These readings were averaged over 10 minute  
166 intervals yielding 732 individual *p*CO<sub>2</sub>, water temperature and pressure values. The CO<sub>2</sub> concentrations in the  
167 Ket River tributaries included between 10 and 20 averaged *p*CO<sub>2</sub> values for each tributary (250 measurements

168 in total) during spring flood period. In addition to continuous *in-situ* CO<sub>2</sub> measurements, we estimated pCO<sub>2</sub>  
169 via measured pH and DIC values, using the set of constants typically applied for riverine pCO<sub>2</sub> estimation in  
170 organic-rich waters (Cai and Wang, 1998; DelDuco and Xu, 2017). The U-test (Mann-Whitney) demonstrated  
171 a lack of significant difference in CO<sub>2</sub> concentrations measured by Vaissala and calculated from the pH and  
172 DIC of the river water.

173 Discrete CO<sub>2</sub> fluxes were measured by using two floating CO<sub>2</sub> chambers equipped with non-  
174 dispersive infrared SenseAir® CO<sub>2</sub> loggers (Bastviken et al., 2015), at each of the 7 (spring flood) and 6  
175 (summer baseflow) sampling location of the main stem and 26 tributaries following the procedures described  
176 elsewhere (Serikova et al., 2019; Krickov et al., 2021). The chambers were not anchored but slowly free-  
177 drifted together with the boat, because it is known that anchored chambers can artificially enhance fluxes due  
178 to turbulence thus providing erroneous estimates (Lorke et al., 2015). The CO<sub>2</sub> accumulation rate inside each  
179 chamber was recorded continuously at 300 s interval. We used first 0.5–1 h of measurements for computing  
180 CO<sub>2</sub> accumulation rate inside each chamber by linear regression.

181 For CH<sub>4</sub> analyses, unfiltered water was sampled in 60-mL Serum bottles. For this, the bottles and caps  
182 were manually submerged at approx. 30 cm depth from the water surface. The bottles were closed without  
183 air bubbles using vinyl stoppers and aluminum caps and immediately poisoned by adding 0.2 mL of saturated  
184 HgCl<sub>2</sub> via a two-way needle system. The samples were stored approximately one week in the refrigerator  
185 before the analyses. In the laboratory, a headspace was created by displacing approximately 40% of water  
186 with N<sub>2</sub> (99.999%). Two 0.5-mL replicates of the equilibrated headspace were analyzed for their  
187 concentrations of CH<sub>4</sub>, using a Bruker GC-456 gas chromatograph (GC) equipped with flame ionization and  
188 thermal conductivity detectors (Serikova et al., 2019; Vorobyev et al., 2021). After every 10 samples, a  
189 calibration of the detectors was performed using Air Liquid gas standards (i.e. 145 ppmv). Duplicate injection  
190 of the samples showed that results were reproducible within ±5%. The specific gas solubility for CH<sub>4</sub>  
191 (Yamamoto et al., 1976) were used in calculation of the CH<sub>4</sub> content in the water. We calculated instantaneous  
192 diffusive CH<sub>4</sub> fluxes for each of the chambers using chamber-specific gas transfer velocity (K<sub>T</sub>) and the  
193 concentrations of dissolved CH<sub>4</sub> in the water and in air-water equilibrium (atm = 1.8 ppm), following the  
194 procedure outlined in Serikova et al. (2018), who used the same setup for measurements of GHG emissions

195 from small and medium-size rivers of the WSL. Note that this setup does not allow measuring the ebullitive  
196 CH<sub>4</sub> fluxes and thus it is possible that the evasion of CH<sub>4</sub>, especially in the stagnant zone of the river flow  
197 and floodplain in this study is sizably underestimated (i.e., Spawn et al., 2015; Stanley et al., 2016; Villa et  
198 al., 2021).

199

### 200 2.3. Chemical analyses of the river water

201 The dissolved oxygen (CellOx 325; accuracy of ±5%), specific conductivity (TetraCon 325; ±1.5%),  
202 and water temperature (±0.2 °C) were measured in-situ at 20 cm depth using a WTW 3320 Multimeter. The  
203 pH was measured using portable Hanna instrument via combined Schott glass electrode calibrated with  
204 standard buffer solutions (4.01, 6.86 and 9.18 at 25°C), with an uncertainty of 0.01 pH units. The temperature  
205 of buffer solutions was within ± 2°C of that of the river water. The water was sampled in pre-cleaned  
206 polypropylene bottle from 20-30 cm depth in the middle of the river and immediately filtered through  
207 disposable single-use sterile Sartorius filter units (0.45 µm pore size). The first 50 mL of filtrate was  
208 discarded. The DOC and Dissolved Inorganic Carbon (DIC) were determined by a Shimadzu TOC-VSCN  
209 Analyzer (Kyoto, Japan) with an uncertainty of 3% and a detection limit of 0.1 mg/L. Blanks of MilliQ water  
210 passed through the filters demonstrated negligible release of DOC from the filter material. The SUVA was  
211 measured via ultraviolet absorbance at 254 nm using a 10-mm quartz cuvette on a Bruker CARY-50 UV-VIS  
212 spectrophotometer.

213 The concentration of C and N in suspended material (Particulate Organic Carbon and Nitrogen (POC  
214 and PON, respectively)) was determined via filtration of 1 to 2 L of freshly collected river water (at the river  
215 bank or in the boat) with pre-weighted GFF filters (47 mm, 0.45 µm) and Nalgene 250-mL polystyrene  
216 filtration units using a Mityvac® manual vacuum pump. Particulate C and N were measured using catalytic  
217 combustion with Cu-O at 900°C with an uncertainty of ≤ 0.5% using Thermo Flash 2000 CN Analyzer at  
218 EcoLab, Toulouse. The samples were analyzed before and after 1:1 HCl treatment to distinguish between  
219 total and inorganic C; however the ratio of C<sub>organic</sub> : C<sub>carbonate</sub> in the river suspended matter (RSM) was always  
220 above 20 and the contribution of carbonate C to total C in the RSM was equal in average 0.3±0.3% (2 s.d., n  
221 = 30).

222 Total microbial cell concentration was measured after sample fixation in glutaraldehyde, by a flow  
223 cytometry (Guava® EasyCyte™ systems, Merck). Cells were stained using 1 µL of a 10 times diluted SYBR  
224 GREEN solution (10000x, Merck), added to 250 µL of each sample before analysis. Particles were identified  
225 as cells based on green fluorescence and forward scatter (Marie et al., 2001).

226

#### 227 *2.4. Riverine carbon export flux by the Ket catchment*

228 The C export flux over active (unfrozen) period (May to October) from the Ket basin was calculated  
229 based on monthly-averaged discharge at the river mouth in 2019 available from Russian Hydrological Survey  
230 and DOC, DIC and POC concentrations measured in the low reaches of the Ket River in this study (see  
231 hydrograph in **Fig. 1**). Riverine element fluxes should be usually estimated using a LOADEST method  
232 (Holmes et al., 2012) from calculated daily element loads. The latter typically obtained from a calibration  
233 regression, applied to daily discharge. This calibration regression can be constructed from time series of  
234 paired streamflow and measured element concentration data for sufficient period of the year. In our previous  
235 works in this and other similar boreal regions, we demonstrated that this method provides reasonable (within  
236 10 to 30 %) agreement with monthly export fluxes calculated by multiplying mean monthly discharge by  
237 mean monthly concentration (Chupakov et al., 2020; Pokrovsky et al., 2022; Vorobyev et al., 2019). Given  
238 that the intrinsic uncertainties on mean monthly discharge are also between 10 and 20 % (see discussion for  
239 the WSL rivers in Pokrovsky et al., 2020), in this study, for open-water period export flux calculation, we  
240 used DOC, DIC and POC concentrations measured during spring flood (for May and June period) and  
241 baseflow (for August, September and October period). For the month of July, we used the mean  
242 concentrations of end of May and August-September which is in accord with seasonal discharge pattern of  
243 the Ket River. Note that the contribution of non-studied October month to total open water period water flux  
244 is < 10 % and thus cannot provide sizable uncertainties

245

246

247

248

249                    *2.5. Landscape parameters and water surface area of the Ket River basin*

250                    The physio-geographical characteristics of the 26 Ket tributaries and the 7 points of the Ket main stem  
251 (**Table S1, Fig. S1**) were determined by applying available digital elevation model (DEM GMTED2010),  
252 soil, vegetation and lithological maps. The landscape parameters were typified using TerraNorte Database of  
253 Land Cover of Russia (Bartalev et al., 2020; <http://terranorte.iki.rssi.ru>). This included various type of forest  
254 (evergreen, deciduous, needleleaf/broadleaf), grassland, tundra, wetlands, water bodies and riparian zones.  
255 Note that the land cover data correspond to the whole catchment area upstream of the sampling point. The  
256 climate parameters the watershed were obtained from CRU grids data (1950-2016) (Harris et al., 2014) and  
257 NCSCD data (Hugelius et al., 2013), respectively. The biomass was obtained from BIOMASAR2 dataset in  
258 raster format with spatial resolution of 1 x 1 km (Santoro et al., 2010). The soil OC content was taken from  
259 the Northern Circumpolar Soil Carbon Database (NCSCD). The original NCSCD dataset produced in GIS  
260 vector format corresponding to 1:1,000,000 scale of topographic map. It could be rasterized to 1 x 1 km pixel  
261 resolution. The lithology layer was taken from GIS version of Geological map of the Russian Federation  
262 (scale 1:5,000,000, <http://www.geolkarta.ru/>). We quantified river water surface area using the global SDG  
263 database with 30 m<sup>2</sup> resolution (Pekel et al., 2016) including both seasonal and permanent water for the open  
264 water period of 2019 and for the multiannual average (reference period 2000-2004). We also used a more  
265 recent GRWL Mask Database which incorporates first order temporary non-active streams (Allen and  
266 Pavelsky, 2018).

267

268                    *2.6. Data analysis*

269                    Carbon concentrations and fluxes for all dataset were tested for normality using a Shapiro-Wilk test.  
270 In case if the data were not normally distributed, we used non-parametric statistics. Comparisons of GHG  
271 parameters in the main stem and tributaries during two sampling seasons were conducted using a non-  
272 parametric Mann Whitney test at a significance level of 0.05. For comparison of unpaired data, a non-  
273 parametric H-criterion Kruskal-Wallis test was used to reveal the differences between different study sites.  
274 The Pearson rank order correlation coefficient ( $p < 0.05$ ) was used to determine the relationship between CO<sub>2</sub>  
275 concentrations and emission fluxes and main landscape parameters of the Ket River tributaries, as well as

276 other potential drivers such as pH, O<sub>2</sub>, water temperature, specific conductivity, DOC, DIC, particulate carbon  
277 and nitrogen, and total bacterial number.

278 Further identification of C pattern drivers in river waters included a Principal Component Analysis  
279 which allowed to test the effect of various hydrochemical and landscape parameters on CO<sub>2</sub> and CH<sub>4</sub>  
280 concentrations and CO<sub>2</sub> emissions. In addition to PCA, a Redundancy analysis (RDA) was used to extract  
281 and summarize the variation in C pattern that can be explained by a set of explanatory variables  
282 (environmental, climatic and hydrochemical factors). The RDA combines a PCA and multiple regression  
283 analysis and it was run in XLSTAT is a statistical software that works as an add-on to Excel.

284

285

### 286 **3. Results**

#### 287 *3.1. Greenhouse gases and dissolved and particulate C*

288 The main hydrochemical parameters and greenhouse gases concentration and exchange fluxes of the  
289 Ket River and its tributaries are listed in **Table 1** and primary data are provided in **Table S2** of the  
290 Supplement. Continuous pCO<sub>2</sub> measurements in the main stem during the spring (764 individual data points  
291 over the full distance of the boat route (834 km) demonstrated a lack of systematic change in CO<sub>2</sub>  
292 concentration from headwaters to the mouth. The CO<sub>2</sub> concentration in tributaries was generally higher than  
293 that in the main stem. As a result, the pCO<sub>2</sub> changed by a factor of 1.5 to 2 when tributaries with high CO<sub>2</sub>  
294 concentrations join the main stem (**Fig. 2 A**). There were strong but non-systematic variations in CO<sub>2</sub>  
295 concentration in the tributaries during the summer (**Fig. 2 C**). The CH<sub>4</sub> concentration (**Table 1 and Fig. S2**  
296 **A, B**) was low in the Ket River (around 0.17 and 0.86 μmol L<sup>-1</sup> in May and August, respectively) and in the  
297 tributaries (range 0.09 to 2.6 μmol L<sup>-1</sup>, 2 to 3 times higher values during the baseflow). These values are  
298 **generally higher than** the range of CH<sub>4</sub> concentration in **large** Siberian Rivers such as Lena (0.03 to 0.199  
299 μmol L<sup>-1</sup>, Bussman, 2013; Vorobyev et al., 2021) **but consistent with concentrations in surface layers of East**  
300 **Siberian ponds (0.6-2.4 μmol L<sup>-1</sup>, Rehder et al., 2021).** In the Ket River main stem and tributaries, the CH<sub>4</sub>  
301 concentrations are 300-2000 and 100-150 times lower than those of CO<sub>2</sub> during spring and summer,

302 respectively, and ranged from 0.05 to 2.0  $\mu\text{mol L}^{-1}$ . Consequently, diffuse  $\text{CH}_4$  emissions (**Table 1, Fig. S2**  
303 **C, D**) constituted 0.1 to 0.5% of total C emissions and are not discussed in further detail.

304 During spring flood,  $\text{CO}_2$  fluxes ranged from 0.26 to 3.2  $\text{g C m}^{-2} \text{d}^{-1}$  in the main stem and tributaries  
305 (**Table 1; Fig. 2 B**). During baseflow, the flux in the tributaries varied from 0.37 to 7.4  $\text{g C m}^{-2} \text{d}^{-1}$  and was a  
306 factor of 2 to 3 higher than that in the main stem (**Fig. 2 D; Table 1**). The  $\text{CO}_2$  concentration in the river  
307 water and gas transfer velocity assessed from discrete measurements by floating chambers ( $K_T = 0.08\text{-}1.83$   
308  $\text{m d}^{-1}$  in the main stem;  $0.2\text{-}1.86 \text{ m d}^{-1}$  in the tributaries, **Table 1**) allowed for calculation of the continuous  
309  $\text{CO}_2$  fluxes (**Fig. 2 B**). For this, we used an average value of  $K_T$  measured between two chamber sites  
310 (separated by a distance of 50 to 100 km) to calculate the  $\text{FCO}_2$  from in-situ measured  $\text{pCO}_2$  in the river  
311 section between these two sites.

312 The DIC concentration increased 5 to 10 times between the spring (2.4 to 2.8  $\text{mg L}^{-1}$ ) and summer  
313 baseflow (18 to 20  $\text{mg L}^{-1}$ ) and the pH increased by 0.5-0.7 units between spring freshet and summer baseflow  
314 (**Fig. 3** and **Fig. S3 A, B** of the Supplement). The DOC concentration ranged from 18 to 25  $\text{mg L}^{-1}$  during  
315 flood and from 15 to 18  $\text{mg L}^{-1}$  during baseflow (**Fig. 3**). There was no systematic variations in DOC  
316 concentration over the 834 km of the main stem ( $20.7 \pm 3.6$  and  $15.0 \pm 1.4 \text{ mg L}^{-1}$  in May and August,  
317 respectively); however, it was slightly higher and more variable in the tributaries ( $22.0 \pm 4.0$  and  $16.5 \pm 7.4$   
318  $\text{mg L}^{-1}$ , **Fig. S3 C, D**). The  $\text{SUVA}_{254}$  remained highly stable throughout the seasons for both the tributaries  
319 and the main stem (range from 4.2 to 4.9  $\text{L mg C}^{-1} \text{m}^{-1}$ , **Table 1**). The POC was 3 times higher during baseflow  
320 compared to spring and ranged from 2 to 10  $\text{mg L}^{-1}$  (**Fig. 3** and **Fig. S3 E, F**). The total bacterial number  
321 ranged from  $5.0 \times 10^5$  to  $8.7 \times 10^5 \text{ cells mL}^{-1}$  for the main stem and tributaries without significant ( $p > 0.05$ )  
322 seasonal variation (**Fig. 3** and **S3 G, H**).

323

### 324 *3.2. Diurnal and spatial variation in $\text{CO}_2$ concentration and flux*

325 The diel (day/night) measurements of  $\text{CO}_2$  concentrations have been performed on six tributaries of  
326 the Ket River during the spring flood period (**Fig. 4**). In two of them (Sochur ad Lopatka), we measured both  
327  $\text{CO}_2$  concentration and  $\text{CO}_2$  fluxes via floating chambers. Continuous  $\text{CO}_2$  concentrations over 10-38 h  
328 exhibited a variation between 5 and 25% of the average value. Only in the case of a small tributary

329 Segondenka (**Fig. 4 E**), when we measured CO<sub>2</sub> over 38 h, there was a local maximum in concentration  
330 between 6 and 7 pm during the first and second day of monitoring, without any significant link to the water  
331 temperature. The deviation of FCO<sub>2</sub> from the average value over the period of observation in two tributaries  
332 (**Fig. 4 A, B**) did not exceed 20%, without any detectable difference between day and night period.

333 The spatial variation in pCO<sub>2</sub> and FCO<sub>2</sub> were tested during spring time in the flood zone of the Ket  
334 River middle course, where the flood zone was connected to the main channel. Regardless of the distance  
335 from the main stem and the size of the water body, the variation in pCO<sub>2</sub> and chamber-based fluxes were  
336 within 30% of the values measured in the main stem. This suggests that the main stem parameters can be used  
337 for upscaling the C emissions to the overall flood plain during May, provided that the water bodies are  
338 connected to the rivers. Further tests of spatial variation were performed on selected small tributaries, when  
339 we moved 8 to 16 km upstream towards the headwaters and monitored the CO<sub>2</sub> concentration in the river  
340 water. There was no sizable trend in CO<sub>2</sub> concentration over several km length of the tributary, consistent  
341 with small fluctuations over the hundred km-scale of the main stem (**Fig. S4 A**). Altogether, rather minor  
342 spatial and diel variations in both CO<sub>2</sub> concentration and emission fluxes support the chosen sampling strategy  
343 and allow reliable extrapolation of obtained results to full surface of lotic waters of the Ket River basin, during  
344 open water period.

345

### 346 *3.3. Impact of water chemistry and catchment characteristics on CO<sub>2</sub> concentrations and emissions*

347 There were generally no strong correlations between CO<sub>2</sub> and CH<sub>4</sub> and the main parameters of the  
348 water column (DOC, DIC, POC, TBC and SUVA (**Table 2**). The CO<sub>2</sub> concentration negatively correlated  
349 with O<sub>2</sub> concentration ( $R_{\text{Pearson}} = -0.68$ ,  $p < 0.05$ ) and FCO<sub>2</sub> positively correlated with SUVA<sub>254</sub> ( $R = 0.34$ ,  $p$   
350  $< 0.05$ ), **Fig. 5 A, B**. Other hydrochemical characteristics of the water column did not impact CO<sub>2</sub> and CH<sub>4</sub>  
351 concentration and CO<sub>2</sub> flux. During spring flood, there was no positive correlation between FCO<sub>2</sub> of the river  
352 water and various hydrochemical characteristics. During the summer baseflow, there were positive  
353 correlations between CO<sub>2</sub> concentration or flux and SUVA and total bacterial number (**Table 2**).

354 There was a decrease in pCO<sub>2</sub> with an increase in the stream order (**Fig. S5 A**), consistent with  
355 negative correlation between pCO<sub>2</sub> and S<sub>watershed</sub> during the spring (**Table 2**). However, neither FCO<sub>2</sub> nor gas

356 transfer coefficient exhibited significant link to the stream order (**Fig. S5 B, C**) or the watershed surface area  
357 (**Table 2**). Among different landscape factors, only deciduous light needleleaf forest (larch trees) exhibited  
358 significant ( $p < 0.01$ ) positive correlations ( $0.6 \leq R_{\text{Pearson}} \leq 0.7$ ) with CO<sub>2</sub> concentration and flux of the Ket  
359 River main stem and tributaries, detectable only during the summer baseflow period (**Fig. 5 C**). The peatland  
360 and bogs at the watershed exhibited only weak, although positive ( $0.2 < R_{\text{Pearson}} < 0.4$ ), correlation with pCO<sub>2</sub>  
361 and FCO<sub>2</sub> (**Table 2**). The other potentially important landscape factors of the river watershed (type of forest,  
362 riparian and total aboveground vegetation, recent burns, water bodies) did not significantly impact the CO<sub>2</sub>  
363 and CH<sub>4</sub> concentration and measured CO<sub>2</sub> fluxes in the Ket River basin (**Table 2**). The mean annual  
364 precipitation (MAP) at the watershed positively correlated with pCO<sub>2</sub> and FCO<sub>2</sub> during the baseflow (**Fig. 5**  
365 **D**).

366 Principal Component Analysis (PCA) demonstrated a general lack of control of physico-chemical  
367 parameters of the water column and watershed land cover on C emission pattern in the river waters. The PCA  
368 identified two factors that had generally low ability to describe the variance (19 and 7%, respectively; **Table**  
369 **S3** of the Supplement). None of the factors acted significantly on dissolved CO<sub>2</sub>, CH<sub>4</sub> or CO<sub>2</sub> flux in the river  
370 water. The RDA treatment did not provide additional insights into environmental control of C pattern across  
371 the rivers and seasons. After normalization, the main result was that the analyses are not statistically  
372 significant ( $p > 0.05$ ).

373

#### 374 *3.4. Areal C emissions and export fluxes*

375 The C emissions ( $> 99.5\%$  CO<sub>2</sub>,  $< 0.5\%$  CH<sub>4</sub>) from the lotic waters of the Ket River basin were  
376 assessed based on total river water coverage of the Ket watershed in 2019 (856 km<sup>2</sup>, of which 691 km<sup>2</sup> is  
377 seasonal water, according to the Global SDG database). Given that the measurements were performed at the  
378 peak of spring flood in 2019, we used the maximal water coverage of the Ket River basin to calculate the  
379 emissions during May and June, and baseflow coverage for measurements during July-October period.

380 For C emission calculation, we used the mean values of FCO<sub>2</sub> of the main stem and the tributaries  
381 ( $1.31 \pm 0.81$  g C m<sup>-2</sup> d<sup>-1</sup> for spring flood;  $2.11 \pm 1.86$  g C m<sup>-2</sup> d<sup>-1</sup> for summer-autumn baseflow) which covers  
382 full variability of both tributaries and the Ket River main channel (**Table 1, Figure 3**). For the month of July

383 which was not sampled in this work and which represents a transition period between the flood and the  
384 baseflow, we used the mean value of May and August ( $1.55 \text{ g C m}^{-2} \text{ d}^{-1}$ ). For the two months of maximal  
385 water flow (May - June), the C emission from the whole Ket basin amounts to  $68 \pm 42 \text{ Gg}$ . When summed up  
386 with July ( $25 \pm 20 \text{ Gg}$ ) and summer-autumn baseflow period (August to October) emission ( $32 \pm 28 \text{ Gg}$ ), the  
387 total open water season emission flux is  $125 \text{ Gg}$ . The uncertainty on the total emission over 6 months of the  
388 open water period is difficult to quantify but it can be estimated as between 30 and 50 %. This range covers  
389 both the uncertainty of the water coverage of the territory (i.e., Krickov et al., 2021) and the seasonal and  
390 spatial variations of  $\text{CO}_2$  emission in the Ket basin assessed in the present study.

391         Based on yield calculations described in section 2.4, the total annual (excluding ice-covered period)  
392 riverine C export from the Ket River basin ( $S_{\text{watershed}} = 94,000 \text{ km}^2$ ) is  $0.35 \text{ Tg}$  ( $3.7 \text{ t C km}^{-2}_{\text{land}} \text{ y}^{-1}$ ), of which  
393 DOC, DIC and POC accounts for 56, 24 and 20%, respectively. Therefore, over the 6 month of open water  
394 period, the C emissions from lotic waters of Ket watershed constituted less than 30% of the dissolved and  
395 particulate downstream export of carbon.

396

397

## 398         **4. DISCUSSION**

### 399         *4.1. Temporal and spatial pattern of $\text{CO}_2$ emissions from the river waters*

400         The first important result of the present study is quite low spatial and seasonal variability in both  $\text{CO}_2$   
401 concentration and emissions, as well as in DOC concentration and aromaticity (reflected by  $\text{SUVA}_{254}$ ) in the  
402 main channel (**Fig. 3, S3, Table 1**). The variability in the tributaries was much larger, with differences in  
403 dissolved and gaseous C parameters between spring flood and summer-autumn baseflow (**Table S4 A**). While  
404  $\text{CO}_2$  concentrations were different between tributaries and the main stem during both flood and baseflow, the  
405  $\text{CO}_2$  flux was not different between the main stem and tributaries regardless of season (**Table S4 B**). This,  
406 together with lack of diel variations in  $\text{CO}_2$  concentrations and emissions during spring period of maximal  
407 water coverage (**Fig. 4**), suggest rather stable pattern of  $\text{CO}_2$  in the river water, not linked to short-scale  
408 processes (primary productivity, photolysis, daily temperature variation). Indeed, negligible primary  
409 productivity in the water column may stem from low water temperatures ( $9.3 \text{ }^\circ\text{C}$ ), shallow photic layer of

410 organic-rich waters (DOC of 22 mg L<sup>-1</sup>) and lack of periphyton activity during high flow of the spring flood.  
411 Note that this finding contrasts the recent results of high frequency pCO<sub>2</sub> measurements in temperate rivers  
412 that show a 30 % higher nocturnal emission compared to daytime observations due to  
413 photosynthesis/respiration cycle (Gómez-Gener et al., 2021b). In the Ambolikha River of Eastern Siberia, a  
414 small (S<sub>watershed</sub> = 121 km<sup>2</sup>) Arctic stream of continuous permafrost zone, the diel CO<sub>2</sub> cycle exhibited a  
415 moderate increase during the day, which was attributed to external lateral sources and photochemical  
416 oxidation of terrestrial DOC, rather than in-stream metabolism (Castro-Morales et al., 2022). At the same  
417 time, several studies in tropical DOM-rich rivers such as Congo (Borges et al. 2019) have not detected diel  
418 variations of CO<sub>2</sub> because aquatic pelagic primary production was low (Descy et al., 2018) due to strong light  
419 attenuation in the water column by DOM.

420 Concerning spatial variability of C concentrations and emissions during the spring flood, the pCO<sub>2</sub>  
421 did not demonstrate sizable variation along the main stem of the Ket River and some of its tributaries, when  
422 moving from the mouth to the headwaters. The SUVA also remained highly stable along the river flow. This,  
423 together with a lack of FCO<sub>2</sub> correlation with river watershed area during this period (Table 2) and the  
424 absence of link between the stream's Strahler order and measured FCO<sub>2</sub> and K<sub>T</sub> (Fig. S5 B, C), suggest  
425 relatively modest control of headwater C cycling by 'fresh' unprocessed organic matter from upland mire  
426 waters on CO<sub>2</sub> emissions from the Ket River basin. Much stronger control of mire waters is reported in boreal  
427 zone of the Northern Europe (Wallin et al., 2013, 2018). Furthermore, our results on the Ket River main stem  
428 and tributaries are in contrast to the general view of disproportional importance of headwater streams in  
429 overall CO<sub>2</sub> emission from river basins (Li et al., 2021). Thus, across the United States fluvial system, the  
430 stream's Strahler order was shown to be important driver of CO<sub>2</sub> evasion from river water surfaces, with  
431 lower order streams exhibiting the highest pCO<sub>2</sub> and gas transfer velocity (Butman and Raymond, 2011). A  
432 likely explanation is relative low values of gas transfer velocity measured in the small streams of the Ket  
433 basin in this study (0.2 - 2.0 m d<sup>-1</sup>, Table 1). Based on a hydraulic model of stream velocity and mean channel  
434 slope (Eqn. 4 in Raymond et al., 2012), we calculated the gas transfer velocities in studied rivers as median  
435 of 1.02, IQR from 0.27 to 1.52 m d<sup>-1</sup>, in very good agreement with chamber-measured values for the Ket  
436 River main stem and tributaries. Although these calculated values are also consistent with transfer coefficients

437 for western Siberia calculated by Liu et al. (2022) based on reach-slope and flow velocity (i.e.,  $K_T \leq 2 \text{ m d}^{-1}$ ), they are typical of lakes rather than rivers (i.e., Kocic et al., 2015). We believe that low  $K_T$  values for the  
438 Ket River basin stem from low channel slope (0.2 to 0.7  $\text{m km}^{-1}$ ) and flow rate (1-2  $\text{km h}^{-1}$ ), strongly forested  
439 and wind-protected river bed without distinct valley due to generally flat orographic context of this part of  
440 the WSL (Serikova et al., 2018). Furthermore, due to small size and short fetch of the Ket River and its  
441 tributaries (see pictures of typical environments in Fig. S4 B-D of the Supplement), extended floodplain zone  
442 also contributes to low values of  $K_T$  measured in the studied river basin. This is consistent with observations  
443 in other flooded regions, where a canopy of vegetation protects the water-air interface from wind stress thus  
444 rendering the gas transfer velocity lower compared to open water such as large river (i.e., Foster-Martinez  
445 and Variano, 2016; Ho et al., 2018; Abril and Borges, 2019). We therefore warn against the use of high value  
446 of transfer velocity, suitable for large Siberian rivers (i.e., Karlsson et al., 2021; Vorobyev et al., 2021), for  
447 assessing the emissions in medium and small size, sheltered streams with extensive riparian vegetation.  
448 Another important aspect linked to C emissions from flooded forest (notably birch trees, see Fig. S4 B) of  
449 the floodplain (e.g. Pangala et al., 2017), not investigated in this study.

451

#### 452 *4.2. Environmental factors possibly controlling CO<sub>2</sub> concentration and emission pattern in the Ket* 453 *River main stem and tributaries*

454 Despite sizable variability of  $\text{pCO}_2$  in the tributaries, especially during the baseflow, there were no  
455 correlations between either  $\text{pCO}_2$  or  $\text{FCO}_2$  and main hydrochemical parameters of the water column (Table  
456 2). The only exception is  $\text{O}_2$  concentration, which negatively correlated with  $\text{pCO}_2$  during spring flood and  
457 both  $\text{pCO}_2$  and  $\text{FCO}_2$  during summer baseflow (Fig. 5 A). This finding suggests potential importance of  
458 shallow suboxic riparian flooded zone, meadows and forest, as well as floodplain lakes, in controlling  $\text{CO}_2$   
459 build up in the water column due to diffusion from sediments or decaying macrophytes, as it was shown for  
460 the floodplain of the Ob River middle course (Krickov et al., 2021). We believe that main reasons of  
461 remarkable stability in  $\text{CO}_2$  concentrations and emissions and weak environmental control on dissolved and  
462 gaseous pattern in the Ket River basin are (1) essentially homogeneous landscapes, lithology and quaternary  
463 deposits of the whole river basin (20-25 % bogs, 60-70% forest, 3-5 % riparian zone), and (2) strong

464 dominance of allochthonous sources in both dissolved and particulate organic matter. Indeed, the SUVA and  
465 bacterial number (TBC) positively correlated with both pCO<sub>2</sub> and FCO<sub>2</sub> during summer (**Fig. 5 B; Table 2**),  
466 which may indicate non-negligible role of bacterial processing of allochthonous (aromatic) DOC delivered  
467 to the water column from wetlands and mires. As such, homogeneous land cover and essentially  
468 allochthonous DOC can still lead to variations of CO<sub>2</sub> per stream size, with small systems showing higher  
469 values than large systems as predicted conceptually (Hotchkiss et al., 2015) and verified at basin-scale (e.g.  
470 Borges et al., 2019). Consistent with this, we observed systematically higher CO<sub>2</sub> concentration and flux in  
471 small tributaries [which were fed by mire waters with ‘non-processed’ OM] compared to the main stem  
472 (**Table 2**). Furthermore, the positive correlation between mean annual precipitation (MAP) and pCO<sub>2</sub> and  
473 FCO<sub>2</sub> during the baseflow (**Table 2, Fig. 5 D**) could reflect the importance of water storage in the mires and  
474 wetlands (which also showed positive but less significant correlations, **Table 2**) during the summer time, and  
475 progressive release of CO<sub>2</sub> and DOC-rich waters from the wetlands to the streams. Another indirect evidence  
476 of the mire water control on CO<sub>2</sub> emission from the river comes from daily CO<sub>2</sub> pattern in a tributary of the  
477 Ket River (**Fig. 4 E**). For this relatively small river ( $S_{\text{watershed}} = 472 \text{ km}^2$ ), we noted that there was quite heavy  
478 rainfall, between 7 am and 3 pm, prior to the CO<sub>2</sub> peak which was observed at 7 pm. Given that water  
479 residence time is very short during spring flood, when the soils are partially frozen, the delivery of  
480 allochthonous DOM and elevated CO<sub>2</sub> from adjacent mires could be the cause of observed CO<sub>2</sub> peak.  
481 Generally, the terrestrial source controlling CO<sub>2</sub> pattern in the Ket River could be either soil litter leachates  
482 (in spring) or bog water (during baseflow, when the river water is substantially derived from wetlands, Ala-  
483 aho et al., 2018a, b). Therefore, the patterns in CO<sub>2</sub> emissions observed in the present study during summer  
484 baseflow thus suggest the importance of allochthonous organic matter from the peatland for CO<sub>2</sub> production  
485 in the water column and in soils where the degradation of DOC is enhanced by the presence of bacteria. This  
486 is consistent with observations in other regions that, during summer-time, numerous processes contribute to  
487 increase CO<sub>2</sub> in rivers such as higher temperature stimulating microbial metabolism, longer residence time  
488 and enhanced flow paths of soil water (Borges et al. 2018).

489 A correlation between CO<sub>2</sub> flux during baseflow and the proportion of deciduous needleleaf forest at  
490 the watershed (**Fig. 5 C**) may suggest the importance of C cycling by larch trees and their possible control on

491 the delivery of degradable organic matter to the river. Similar control of larch vegetation on riverine CO<sub>2</sub> has  
492 been suggested for the Lena River, Eastern Siberia (Vorobyev et al., 2021) although we acknowledge that  
493 further observations on contrasted Siberian watersheds are necessary to confirm the observation that larch  
494 trees litterfall led to export of degradable OM to the river.

495 In the Ket River basin, the local soil/groundwater effects are expected to be more pronounced during  
496 baseflow, due to lower impact of dilution, compared to the spring flood period. The hypothesis of deeper flow  
497 path in summer compared to spring is confirmed for the WSL (Frey and McClelland, 2009; Pokrovsky et al.,  
498 2015; Serikova et al., 2018) and is supported in this study by a strong increase in DIC concentration between  
499 spring and summer (**Fig. 3**). Thus, although the pairwise correlations between parameters do not support any  
500 particular mechanism, it is not excluded that OM bio- and photo degradation and local mire water feeding  
501 drive FCO<sub>2</sub> in spring, and that deeper flowpaths and DIC export drive the elevated FCO<sub>2</sub> in summer. The  
502 latter is consistent with results of analysis of streams and rivers across the contiguous United States, which  
503 demonstrated that ~60% of CO<sub>2</sub> evasion is from external sources rather than internal production (Hotchkiss  
504 et al., 2015). In view of lack of correlation of CO<sub>2</sub> emissions in the Ket River and tributaries with  
505 hydrochemical parameters of the water column, we believe that external source of CO<sub>2</sub> in studied river system  
506 represents sizable contribution to total riverine CO<sub>2</sub> evasion across the seasons and sampling sites. In  
507 particular, in small peatland streams, the CO<sub>2</sub>-rich deep peat/groundwater is known to be the major source of  
508 aquatic CO<sub>2</sub> under low flow conditions (Dinsmore and Billett, 2008), whereas in boreal headwater streams  
509 of N Sweden the main source of stream CO<sub>2</sub> was inflowing CO<sub>2</sub>-rich soil waters (Winterdahl et al., 2016).

510 Another important factor responsible for higher CO<sub>2</sub> production in the water column in summer  
511 compared to spring could be POC degradation. The riverine POC is known to be much more biodegradable  
512 than DOC (Attermeyer et al., 2018), and the POC concentration in the Ket River basin increased 4-fold  
513 between spring and summer (**Table 1**). The origin of summer-time POC and its lability remain elusive, but  
514 could be a combination of plankton bloom and mire- or forest-derived DOC coagulation products in the water  
515 column (Krickov et al., 2018). Furthermore, pronounced heterogeneity in CO<sub>2</sub> emission during baseflow  
516 among tributaries may also reflect the heterogeneity of riverine organic matter which is known to be the  
517 maximal during low flow conditions and minimal during high flow (Lynch et al., 2019).

518 The main unexpected result of this study is that none of the physiochemical parameters of the water  
519 column and the land cover factor is sufficiently strong to drive the CO<sub>2</sub> and CH<sub>4</sub> patterns, although they show  
520 pronounced spatial and seasonal variations. Although correlations do not necessary imply causation and some  
521 correlations could be spurious or indirect, this analysis, together with PCA treatment, allow first order  
522 assessment of possible governing factors or dismissing the environmental parameters that do not contribute  
523 in GHG pattern control. A likely explanation is that simultaneous operation of multiple aquatic processes that  
524 include carbon, oxygen, nutrient, and plankton and peryphyton dynamics as well as sediment respiration  
525 control the CO<sub>2</sub> and CH<sub>4</sub> exchanges with the atmosphere, as it is known for boreal lakes and floodplain zones  
526 of the boreal rivers (i.e., Bayer et al., 2019; Zabelina et al., 2021; Krickov et al., 2019). Given that even a  
527 multiparametric statistical treatment (PCA) did not demonstrate sizable explanation capacity of the data set,  
528 we cannot exclude that these potential physico-chemical, microbiological and landscape drivers are working  
529 in different (opposing) directions and have counteracted each other. However, further in-depth analysis of  
530 these interactions requires much better seasonal resolution, ideally over full period of the year, which was  
531 beyond the scope of the present study.

532

#### 533 *4.3. Emissions from the Ket River basin compared to downstream export of riverine carbon*

534 The estimated C emissions (> 99.5 % C; < 0.5 % CH<sub>4</sub>) from the Ket River main channel over 830 km  
535 distance (0.5 to 2.5 g C m<sup>-2</sup> d<sup>-1</sup>) are comparable to those of the Ob River main channel (1.32±0.14 g C m<sup>-2</sup> d<sup>-1</sup>  
536 <sup>1</sup> in the permafrost-free zone; Karlsson et al., 2021). The CO<sub>2</sub> emission in Ket's tributaries (1 to 2 g C m<sup>-2</sup> d<sup>-1</sup>  
537 <sup>1</sup> in spring; 1 to 5 g C m<sup>-2</sup> d<sup>-1</sup> in summer) are within the range reported for small rivers and streams of the  
538 permafrost-free zone of western Siberia (0 to 3.6 g C m<sup>-2</sup> d<sup>-1</sup> in spring; 4 to 9 g C m<sup>-2</sup> d<sup>-1</sup> in summer; Serikova  
539 et al., 2018), forest and wetland headwater streams of northern Sweden (0.5 to 5 g C m<sup>-2</sup> d<sup>-1</sup>; Gómez-Gener  
540 et al., 2021a), and boreal streams in Canada and Alaska (0.8 to 5.2 g C m<sup>-2</sup> d<sup>-1</sup>, Koprivnjak et al., 2010;  
541 Teodoru et al., 2009; Crawford et al., 2013; Campeau et al., 2014). Total C emissions from the water surfaces  
542 of the Ket River basin assessed in this study (148 g C-CO<sub>2</sub> m<sup>-2</sup><sub>water</sub> y<sup>-1</sup>, assuming no emission under ice), when  
543 normalized to the Ket river basin area (S<sub>watershed</sub> = 94,000 km<sup>2</sup>), amounts to 1.35 g C m<sup>-2</sup><sub>land</sub> y<sup>-1</sup>. Generally  
544 higher land area - specific emissions, comparable or exceeding those of the Ket River, were reported in

545 Québec (1.0 to 4.6 g C m<sup>-2</sup> y<sup>-1</sup>; Campeau and del Giorgio, 2014; Hutchins et al., 2019; Teodoru et al., 2009),  
546 Sweden (1.6 to 8.6 g C m<sup>-2</sup> y<sup>-1</sup>; Humborg et al., 2010; Jonsson et al., 2007; Lundin et al., 2013; Wallin et al.,  
547 2011, 2018) and boreal portions of the Yukon River (7 to 9 g C m<sup>-2</sup> y<sup>-1</sup>; Striegl et al., 2012; Stackpoole et al.,  
548 2017). Possible reasons for these differences could be different areal coverage of the territory by river  
549 network, the calculated rather than measured CO<sub>2</sub> fluxes, or the higher gas transfer velocity in the rivers from  
550 mountainous regions.

551 The regional assessment of the Ket River basin performed in this study are based on direct chamber  
552 measurements of emissions and as such provide rigorous basis for upscaling the CO<sub>2</sub> emissions from currently  
553 understudied lotic waters of permafrost-free zone of Western Siberia. The C evasion from the fluvial network  
554 of the Ket River assessed in the present work (127 ± 11 Gg y<sup>-1</sup>, ignoring the emission during the ice breakup  
555 in early spring) is 3 times lower than the total (DOC+DIC+POC) downstream export by this river from the  
556 same territory (0.35 Tg C y<sup>-1</sup>). The riverine C yield for the Ket River (3.7 t C km<sup>-2</sup><sub>land</sub> y<sup>-1</sup>) is in agreement  
557 with regional C (DOC+DIC) yield by permafrost-free small and medium size rivers of the WSL (3 to 4 t C  
558 km<sup>-2</sup><sub>land</sub> y<sup>-1</sup>, Pokrovsky et al., 2020) and with the Ob River in the permafrost-free zone (3.6 t C km<sup>-2</sup><sub>land</sub> y<sup>-1</sup>,  
559 Vorobyev et al., 2019). Note that the latter study of the Ob River, which is very similar in the environmental  
560 context to the Ket River, included high frequency weekly sampling over several years of monitoring. Thus,  
561 the similarity of downstream export fluxes of the Ket and Ob Rivers support the validity of approaches for  
562 sampling and C yield calculation employed in the present study. Such high C yields in the southern,  
563 permafrost-free part of the WSL stem from essentially inorganic carbon originated from groundwater  
564 discharge of carbonate mineral rich reservoirs, abundant in this region (Pokrovsky et al., 2015). At the same  
565 time, the organic C yield in rivers of this region is quite low and represents less than 20 % of total C yield  
566 (Pokrovsky et al., 2020; Vorobyev et al., 2019). This can explain anomalously low value of C evasion : C  
567 export of the Ket River (1 : 3) measured in this work as compared to the average values for permafrost-free  
568 zone of Western Siberia (1 : 1, Serikova et al., 2019). Another factor potentially leading to underestimation  
569 of C evasion in this study is GIS-based minimal water coverage which does not include seasonal oxbow lakes,  
570 flooded forest and temporary water bodies of the floodplain which provide sizable emissions (see Krickov et  
571 al., 2021). We also do not exclude that some important hot moments / hot spots of C emission were missed

572 in our sampling campaign, such as summer baseflow/autumn peaks (Serikova et al., 2019) or stagnant zones  
573 of the floodplain in summer (Krickov et al., 2021; Castro-Morales et al., 2021). This calls a need for higher  
574 spatial and temporal resolution monitoring of C emission, with special focus on important events across full  
575 hydrological continuum.

576

577

## 578 **5. Concluding remarks**

579 Via combination of discrete floating chamber and hydrochemistry and continuous CO<sub>2</sub> concentration  
580 measurements over 830 km of large pristine boreal river of western Siberia main channel and its 26 tributaries  
581 during the peak of spring flood and the summer-autumn baseflow, we quantified spatial and temporal  
582 variations, overall emissions of C (CO<sub>2</sub>, CH<sub>4</sub>) and export of (DOC, DIC and POC) during the 6 months of  
583 open water period. The range of CO<sub>2</sub> and CH<sub>4</sub> concentrations in the main channel and tributaries as well as  
584 CO<sub>2</sub> emissions were consistent with other boreal and subarctic regions but demonstrated rather low seasonal  
585 and spatial variability. The diel CO<sub>2</sub> flux by floating chambers and continuous pCO<sub>2</sub> measurements in the  
586 tributaries of the Ket River during spring flood demonstrated negligible impact of day/night period on the  
587 CO<sub>2</sub> concentrations and emission fluxes.

588 We hypothesize that homogeneous landscape coverage (bog and taiga forest) provide stable  
589 allochthonous input of DOM as confirmed by very weak spatial and seasonal variations of DOM aromaticity.  
590 Among possible driving factors of CO<sub>2</sub> production in the water column (bio- and photo-degradation of DOC  
591 and POC, plankton metabolism), none seems to be sizably important for persistent CO<sub>2</sub> supersaturation and  
592 relevant emissions. The landscape factors of the watershed (bog and forest coverage, soil organic carbon  
593 stock) of the tributaries and along the main stem did not sizably affected the C concentration and emission  
594 pattern across two seasons. We hypothesize that stable terrestrial input of strongly aromatic DOM, shallow  
595 photic layer and humic waters of the Ket River basin preclude sizable daily and seasonal variations of C  
596 parameters. Punctual discharge of groundwater, resuspension of sediments or shallow subsurface influx from  
597 mires and riparian zone may be responsible for small-scale heterogeneities in C emissions and concentrations  
598 along the main stem and among the tributaries. These effects are much stronger pronounced during summer

599 baseflow compared to spring flood. Overall, deeper flow paths in summer compared to spring enhance the  
600 DIC discharge within the river bed and the tributaries, thus leading to elevated CO<sub>2</sub> flux in summer.  
601 Additional factor responsible for higher CO<sub>2</sub> emission during this season could be mire-originated particulate  
602 organic matter (POM) processing in the water column.

603 The six month open-water period C emissions from the lotic waters of the Ket River basin were sizably  
604 lower than the downstream total C export by this river during the same period. We conclude that regional  
605 estimations of C balance in lotic systems should be based on a combination of direct chamber measurements,  
606 discrete hydrochemical sampling and continuous in-situ monitoring with submersible sensors, at least during  
607 two most important hydrological periods of the year which are, for boreal regions, the spring flood and the  
608 summer-autumn baseflow. We believe that this is the best trade-off between scientific rigor and logistical  
609 feasibility in poorly accessible, pristine and strongly understudied regions.

610

#### 611 **Acknowledgements.**

612 We acknowledge support from RSF grant 22-17-00253, the TSU Development Program “Priority-2030”,  
613 and the Swedish Research Council (grant no. 2016-05275).

614

#### 615 **Authors contribution.**

616 AL and OP designed the study and wrote the paper; AL, SV, IK and OP performed sampling, analysis and  
617 their interpretation; LS performed bacterial assessment and DOC/DIC analysis and interpretation; MK  
618 performed landscape characterization of the Ket River basin and calculated water surface area; SK  
619 performed hydrological analysis; JK provided analyses of literature data, transfer coefficients for FCO<sub>2</sub>  
620 calculations and global estimations of areal emission vs export.

621

#### 622 **Competing interests.**

623 The authors declare that they have no conflict of interest.

624

#### 625 **Data availability.**

626 Pokrovsky, O., Lim, A., Krickov, I., Korets, M., Vorobyev, S.: “Ket River hydrochemistry, CO<sub>2</sub> concentration  
627 and landscape parameters”, Mendeley Data, V1, doi: 10.17632/snwbkvg6tc.1, 2022.

628

#### 629 **References**

- 630 Abril, G., Martinez, J.-M., Artigas, L. F., Moreira-Turcq, P., Benedetti, M. F., Vidal, L., Meziane, T., Kim,  
631 J.-H., Bernardes, M. C., Savoye, N., Deborde, J., Albéric, P., Souza, M. F. L., Souza, E. L., and Roland,  
632 F.: Amazon river carbon dioxide outgassing fueled by wetlands, *Nature*, 505, 395-398,  
633 <https://doi.org/10.1038/nature12797>, 2014.
- 634 Abril, G. and Borges, A. V.: Ideas and perspectives: Carbon leaks from flooded land: do we need to replumb  
635 the inland water active pipe? *Biogeosciences*, 16, 769–784, <https://doi.org/10.5194/bg-16-769-2019>,  
636 2019.
- 637 Ala-Aho, P., Soulsby, C., Pokrovsky, O. S., Kirpotin, S. N., Karlsson, J., Serikova, S., Manasypov, R., Lim,  
638 A., Krickov, I., Kolesnichenko, L. G., Laudon, H., and Tetzlaff, D.: Permafrost and lakes control river  
639 isotope composition across a boreal Arctic transect in the Western Siberian lowlands, *Environ. Res.*  
640 *Lett.*, 13, <https://doi.org/10.1088/1748-9326/aaa4fe>, 2018a.
- 641 Ala-aho, P., Soulsby, C., Pokrovsky, O. S., Kirpotin, S. N., Karlsson, J., Serikova, S., Vorobyev, S. N.,  
642 Manasypov, R. M., Loiko, S., and Tetzlaff, D.: Using stable isotopes to assess surface water source  
643 dynamics and hydrological connectivity in a high-latitude wetland and permafrost influenced  
644 landscape, *J. Hydrol.*, 556, 279–293, <https://doi.org/10.1016/j.jhydrol.2017.11.024>, 2018b.
- 645 Alin, S. R., Rasera, M. D. F. F. L., Salimon, C. I., Richey, J. E., Holtgrieve, G. W., Krusche, A. V., and  
646 Snidvongs, A.: Physical controls on carbon dioxide transfer velocity and flux in low-gradient river  
647 systems and implications for regional carbon budgets, *J. Geophys. Res. Biogeosciences*, 116,  
648 <https://doi.org/10.1029/2010JG001398>, 2011.
- 649 Allen, G. H. and Pavelsky, T. M.: Global extent of rivers and streams, *Science*, 361, 585–588,  
650 <https://doi.org/10.1126/science.aat0636>, 2018.
- 651 Almeida, R. M., Pacheco, F. S., Barros, N., Rosi, E., and Roland, F.: Extreme floods increase CO<sub>2</sub> outgassing  
652 from a large Amazonian river, *Limnol. Oceanogr.*, 62, 989–999, <https://doi.org/10.1002/lno.10480>,  
653 2017.
- 654 Amaral, J. H. F., Borges, A. V., Melack, J. M., Sarmiento, H., Barbosa, P. M., Kasper, D., Melo, M. L., de  
655 Fex Wolf, D., da Silva, J. S., and Forsberg, B. R.: Influence of plankton metabolism and mixing  
656 depth on CO<sub>2</sub> dynamics in an Amazon floodplain lake, *Sci. Total. Env.* 630, 1381-1393,  
657 <https://doi.org/10.1016/j.scitotenv.2018.02.331>, 2018.
- 658 Amaral, J. H. F., Melack, J. M., Barbosa, P. M., Borges, A. V., Kasper, D., Cortes, A. C., Zhou, W.,  
659 MacIntyre, S., and Forsberg, B. R.: Inundation, hydrodynamics and vegetation influences carbon  
660 dioxide concentrations in Amazon floodplain lakes, *Ecosystems*, 25(4), 911–930,  
661 <https://doi.org/10.1007/s10021-021-00692-y>, 2022.
- 662 Attermeyer, K., Catalán, N., Einarsdottir, K., Freixa, A., Groeneveld, M., Hawkes, J. A., Bergquist, J., and  
663 Tranvik, L. J.: Organic carbon processing during transport through boreal inland waters: particles as  
664 important sites, *J. Geophys. Res. Biogeosciences*, 123, 2412–2428,  
665 <https://doi.org/10.1029/2018JG004500>, 2018.
- 666 Bartalev, S. A., Egorov, V. A., Ershov, D. V., Isaev, A. S., Lupyan, E. A., Plotnikov, D. E., and Uvarov, I.  
667 A.: Remote mapping of vegetation land cover of Russia based on data of MODIS spectroradiometer,  
668 *Mod. Probl. Earth Remote Sens. Space*, 8, 285–302, 2018.
- 669 Bastviken, D., Sundgren, I., Natchimuthu, S., Reyier, H., and Gålfalk, M.: Technical Note: Cost-efficient  
670 approaches to measure carbon dioxide (CO<sub>2</sub>) fluxes and concentrations in terrestrial and aquatic  
671 environments using mini loggers, *Biogeosciences*, 12, 3849–3859, [https://doi.org/10.5194/bg-12-3849-](https://doi.org/10.5194/bg-12-3849-2015)  
672 2015, 2015.
- 673 Bayer, T. K., Gustafsson, E., Brakebusch, M., and Beer, C.: Future carbon emission from boreal and  
674 permafrost lakes are sensitive to catchment organic carbon loads, *J. Geophys. Res. Biogeosciences*,  
675 124, 1827-1848, <https://doi.org/10.1029/2018JG004978>, 2019.
- 676 Borges, A. V., Darchambeau, F., Lambert, T., Bouillon, S., Morana, C., Brouyère, S., Hakoun, V., Jurado,  
677 A., Tseng, H-C., Descy, J.-P., and Roland, F. A. E.: Effects of agricultural land use on fluvial carbon  
678 dioxide, methane and nitrous oxide concentrations in a large European river, the Meuse (Belgium),  
679 *Sci. Total Environ.*, 610-611, 342-355, <https://doi.org/10.1016/j.scitotenv.2017.08.047>, 2018.
- 680 Borges, A. V., Darchambeau, F., Teodoru, C. R., Marwick, T. R., Tamoo, F., Geeraert, N., Omengo, F. O.,  
681 Guérin, F., Lambert, T., Morana, C., Okuku, E., and Bouillon, S.: Globally significant greenhouse gas

- 682 emissions from African inland waters, *Nature Geoscience*, 8, 637–642,  
683 <https://doi.org/10.1038/NGEO2486>, 2015.
- 684 Bussmann, I.: Distribution of methane in the Lena Delta and Buor-Khaya Bay, Russia, *Biogeosciences*, 10,  
685 4641–4652, <https://doi.org/10.5194/bg-10-4641-2013>, 2013.
- 686 Butman, D. and Raymond, P.: Significant efflux of carbon dioxide from streams and rivers in the United  
687 States, *Nature Geoscience*, 4, 839–842. <https://doi.org/10.1038/ngeo1294>, 2011.
- 688 Cai, W.-J. and Wang, Y.: The chemistry, fluxes, and sources of carbon dioxide in the estuarine waters of the  
689 Satilla and Altamaha Rivers, Georgia, *Limnol. Oceanogr.*, 43, 657–668,  
690 <https://doi.org/10.4319/lo.1998.43.4.0657>, 1998.
- 691 Campeau, A. and del Giorgio, P. A.: Patterns in CH<sub>4</sub> and CO<sub>2</sub> concentrations across boreal rivers: Major  
692 drivers and implications for fluvial greenhouse emissions under climate change scenarios, *Glob.  
693 Change Biol.*, 20, 1075–1088, <https://doi.org/10.1111/gcb.12479>, 2014.
- 694 Campeau, A., Lapierre, J.-F., Vachon, D., and del Giorgio, P. A.: Regional contribution of CO<sub>2</sub> and CH<sub>4</sub>  
695 fluxes from the fluvial network in a lowland boreal landscape of Québec, *Glob. Biogeochem. Cycles*,  
696 28, 57–69, <https://doi.org/10.1002/2013GB004685>, 2014.
- 697 Castro-Morales, K., Canning, A., Körtzinger, A., Göckede, M., Küsel, K., Overholt, W. A., Wichard, T.,  
698 Redlich, S., Arzberger, S., Kolle, O., and Zimov, N.: Effects of reversal of water flow in an Arctic  
699 floodplain river on fluvial emissions of CO<sub>2</sub> and CH<sub>4</sub>, *J. Geophys. Res. Biogeosciences*, 127,  
700 e2021JG006485, <https://doi.org/10.1029/2021JG006485>, 2022.
- 701 Chadburn, S. E., Krinner, G., Porada, P., Bartsch, A., Beer, C., Beleggi Marchesini, L., Boike, J., Ekici, A.,  
702 Elberling, B., Friborg, T., Hugelius, G., Johansson, M., Kuhry, P., Kutzbach, L., Langer, M., Lund, M.,  
703 Parmentier, F.-J. W., Peng, S., Van Huissteden, K., Wang, T., Westermann, S., Zhu, D., and Burke, E.  
704 J.: Carbon stocks and fluxes in the high latitudes: using site-level data to evaluate Earth system models,  
705 *Biogeosciences*, 14, 5143–5169, <https://doi.org/10.5194/bg-14-5143-2017>, 2017.
- 706 Cooper, L. W., McClelland, J. W., Holmes, R. M., Raymond, P. A., Gibson, J. J., Guay, C. K., and Peterson,  
707 B. J.: Flow-weighted values of runoff tracers ( $\delta^{18}\text{O}$ , DOC, Ba, alkalinity) from the six largest Arctic  
708 rivers, *Geophys. Res. Lett.*, 35, L18606, <https://doi.org/10.1029/2008GL035007>, 2008.
- 709 Crawford, J. T., Striegl, R. G., Wickland, K. P., Dornblaser, M. M., and Stanley, E. H.: Emissions of carbon  
710 dioxide and methane from a headwater stream network of interior Alaska, *J. Geophys. Res.  
711 Biogeosciences*, 118, 482–494, <https://doi.org/10.1002/jgrg.20034>, 2013.
- 712 Crawford, J. T., Loken, L. C., Casson, N. J., Smith, C., Stone, A. G., and Winslow, L. A.: High-speed  
713 limnology: using advanced sensors to investigate spatial variability in biogeochemistry and hydrology,  
714 *Environ. Sci. Technol.*, 49, 442–450, <https://doi.org/10.1021/es504773x>, 2015.
- 715 Crawford, J. T., Stanley, E. H., Dornblaser, M. M., and Striegl, R. G.: CO<sub>2</sub> time series patterns in  
716 contrasting headwater streams of North America, *Aquatic Sciences*, 79, 473–  
717 486, <https://doi.org/10.1007/s00027-016-0511-2>, 2016a.
- 718 Crawford, J. T., Loken, L. C., Stanley, E. H., Stets, E. G., Dornblaser, M. M., and Striegl, R. G.: Basin scale  
719 controls on CO<sub>2</sub> and CH<sub>4</sub> emissions from the Upper Mississippi River, *Geophys. Res. Lett.*, 43, 1973–  
720 1979, <https://doi.org/10.1002/2015GL067599>, 2016b.
- 721 Crawford, J. T., Butman, D. E., Loken, L. C., Stadler, P., Kuhn, C., and Striegl, R. G.: Spatial variability of  
722 CO<sub>2</sub> concentrations and biogeochemistry in the Lower Columbia River, *Inland Waters*, 7, 417–427,  
723 <https://doi.org/10.1080/20442041.2017.1366487>, 2017.
- 724 Dawson, J. J., Billett, M. F., Hope, D., Palmer, S. M., and Deacon, C.: Sources and sinks of aquatic carbon  
725 in a peatland stream continuum, *Biogeochemistry*, 70, 71–92, 2004.
- 726 Descy, J. P., Darchambeau, F., Lambert, T., Stoyneva, M. P., Bouillon, S., and Borges, A. V.: Phytoplankton  
727 dynamics in the Congo River, *Freshwater Biology*, 62, 87–101, <https://doi.org/10.1111/fwb.12851>,  
728 2017.
- 729 DelDuco, E. M. and Xu, Y. J.: Dissolved carbon transport and processing in North America’s largest swamp  
730 river entering the Northern Gulf of Mexico, *Water*, 11, 1395, <https://doi.org/10.3390/w11071395>, 2019.
- 731 Denfeld, B. A., Frey, K. E., Sobczak, W. V., Mann, P. J., and Holmes, R. M.: Summer CO<sub>2</sub> evasion from  
732 streams and rivers in the Kolyma River basin, north-east Siberia, *Polar Res.*, 32, 19704,  
733 <https://doi.org/10.3402/polar.v32i0.19704>, 2013.

734 Dinsmore, K. J. and Billett, M. F.: Continuous measurement and modeling of CO<sub>2</sub> losses from a peatland  
735 stream during stormflow events, *Water Resour. Res.*, 44, W12417,  
736 <https://doi.org/10.1029/2008WR007284>, 2008.

737 Dinsmore, K. J., Billett, M. F., and Dyson, K. E.: Temperature and precipitation drive temporal variability in  
738 aquatic carbon and GHG concentrations and fluxes in a peatland catchment, *Glob. Change Biol.*, 19,  
739 2133–2148, <https://doi.org/10.1111/gcb.12209>, 2013.

740 Feng, X., Vonk, J. E., Dongen, B. E. V., Gustafsson, Ö., Semiletov, I. P., Dudarev, O. V., Wang, Z.,  
741 Montluçon, D. B., Wacker, L., and Eglinton, T. I.: Differential mobilization of terrestrial carbon pools  
742 in Eurasian Arctic river basins, *Proc. Natl. Acad. Sci. U. S. A.*, 110, 14168–14173,  
743 <https://doi.org/10.1073/pnas.1307031110>, 2013.

744 Foster-Martinez, M. R. and Variano, E. A.: Air-water gas exchange by waving vegetation stems, *J. Geophys.*  
745 *Res. Biogeosciences*, 121, 1916–1923, <https://doi.org/10.1002/2016JG003366>, 2016.

746 Frey, K. E. and Smith, L. C.: How well do we know northern land cover? Comparison of four global  
747 vegetation and wetland products with a new ground-truth database for West Siberia. *Glob. Biogeochem.*  
748 *Cycles*, 21, GB1016. <https://doi.org/10.1029/2006GB002706>, 2007.

749 Frey, K. E. and McClelland, J. W.: Impacts of permafrost degradation on arctic river biogeochemistry,  
750 *Hydrol. Process.*, 23, 169–182, <https://doi.org/10.1002/hyp.7196>, 2009.

751 Gómez-Gener, L., Rocher-Ros, G., Battin, T., Cohen, M. J., Dalmagro, H. J., Dinsmore, K. J., Drake, T. W.,  
752 Duvert, C., Enrich-Prast, A., Horgby, Å., Johnson, M. S., Kirk, L., Machado-Silva, F., Marzolf, N. S.,  
753 McDowell, M. J., McDowell, W. H., Miettinen, H., Ojala, A. K., Peter, H., Pumpanen, J., Ran, L.,  
754 Riveros-Iregui, D. A., Santos, I. R., Six, J., Stanley, E. H., Wallin, M. B., White, S. A., and Sponseller,  
755 R. A.: Global carbon dioxide efflux from rivers enhanced by high nocturnal emissions, *Nat. Geosci.*,  
756 1–6, <https://doi.org/10.1038/s41561-021-00722-3>, 2021a.

757 Gómez-Gener, L., Hotchkiss, E. R., Laudon, H., and Sponseller, R. A.: Integrating discharge-concentration  
758 dynamics across carbon forms in a boreal landscape, *Water Resour. Res.*, 57, e2020WR028806,  
759 <https://doi.org/10.1029/2020WR028806>, 2021b.

760 Griffin, C. G., McClelland, J. W., Frey, K. E., Fiske, G., and Holmes, R. M.: Quantifying CDOM and DOC  
761 in major Arctic rivers during ice-free conditions using Landsat TM and ETM+ data, *Remote Sens.*  
762 *Environ.*, 209, 395–409, <https://doi.org/10.1016/j.rse.2018.02.060>, 2018.

763 Harris, I., Jones, P. d., Osborn, T. j., and Lister, D. h.: Updated high-resolution grids of monthly climatic  
764 observations – the CRU TS3.10 Dataset, *Int. J. Climatol.*, 34, 623–642,  
765 <https://doi.org/10.1002/joc.3711>, 2014.

766 Ho, D. T., Engel, V. C., Ferrón, S., Hickman, B., Choi, J., and Harvey, J. W.: On factors influencing air-water  
767 gas exchange in emergent wetlands, *J. Geophys. Res. Biogeosciences*, 123, 178–192,  
768 <https://doi.org/10.1002/2017JG004299>, 2018.

769 Holmes, R. M., McClelland, J. W., Peterson, B.J., & Tank S. E. et al. Seasonal and annual fluxes of nutrients  
770 and organic matter from large rivers to the Arctic Ocean and surrounding seas, *Estuaries and Coasts*,  
771 35, 369–382. doi: 10.1007/s12237-011-9386-6, 2012.

772 Holmes, R. M., Coe, M. T., Fiske, G. J., Gurtovaya, T., McClelland, J. W., Shiklomanov, A. I., Spencer, R.  
773 G. M., Tank, S. E., and Zhulidov, A. V.: Climate change impacts on the hydrology and biogeochemistry  
774 of Arctic Rivers, in: *Climatic Changes and Global warming of Inland Waters: Impacts and Mitigation*  
775 *for Ecosystems and Societies*, edited by: Goldman, C. R., Kumagi, M., and Robarts, R. D., John Wiley  
776 and Sons, 1–26, 2013.

777 Hotchkiss, E. R., Hall Jr, R. O., Sponseller, R. A., Butman, D., Klaminder, J., Laudon, H., Rosvall, M., and  
778 Karlsson, J.: Sources of and processes controlling CO<sub>2</sub> emissions change with the size of streams and  
779 rivers, *Nat. Geosci.*, 8, 696–699, <https://doi.org/10.1038/ngeo2507>, 2015.

780 Hugelius, G., Tarnocai, C., Broll, G., Canadell, J. G., Kuhry, P., and Swanson, D. K.: The northern  
781 circumpolar soil carbon database: Spatially distributed datasets of soil coverage and soil carbon storage  
782 in the northern permafrost regions, *Earth Syst. Sci. Data*, 5, 3–13, [https://doi.org/10.5194/essd-5-3-](https://doi.org/10.5194/essd-5-3-2013)  
783 2013, 2013.

784 Humborg, C., Mörth, C.-M., Sundbom, M., Borg, H., Blenckner, T., Giesler, R., and Ittekkot, V.: CO<sub>2</sub>  
785 supersaturation along the aquatic conduit in Swedish watersheds as constrained by terrestrial

786 respiration, aquatic respiration and weathering, *Glob. Change Biol.*, 16, 1966–1978,  
787 <https://doi.org/10.1111/j.1365-2486.2009.02092.x>, 2010.

788 Hutchins, R. H. S., Prairie, Y. T., and del Giorgio, P. A.: Large-Scale Landscape Drivers of CO<sub>2</sub>, CH<sub>4</sub>, DOC,  
789 and DIC in Boreal River Networks, *Glob. Biogeochem. Cycles*, 33, 125–142,  
790 <https://doi.org/10.1029/2018GB006106>, 2019.

791 Hutchins, R. H. S., Tank, S. E., Olefeldt, D., Quinton, W. L., Spence, C., Dion, N., Estop-Aragonés, C., and  
792 Mengistu, S. G.: Fluvial CO<sub>2</sub> and CH<sub>4</sub> patterns across wildfire-disturbed ecozones of subarctic Canada:  
793 Current status and implications for future change, *Glob. Change Biol.*, 26, 2304–2319,  
794 <https://doi.org/10.1111/gcb.14960>, 2020.

795 Johnson, M. S., Billett, M. F., Dinsmore, K. J., Wallin, M., Dyson, K. E., and Jassal, R. S.: Direct and  
796 continuous measurement of dissolved carbon dioxide in freshwater aquatic systems—method and  
797 applications, *Ecohydrology*, 3, 68–78, <https://doi.org/10.1002/eco.95>, 2009.

798 Jonsson, A., Algesten, G., Bergström, A.-K., Bishop, K., Sobek, S., Tranvik, L. J., and Jansson, M.:  
799 Integrating aquatic carbon fluxes in a boreal catchment carbon budget, *J. Hydrol.*, 334, 141–150,  
800 <https://doi.org/10.1016/j.jhydrol.2006.10.003>, 2007.

801 Karlsson, J., Serikova, S., Vorobyev, S. N., Rocher-Ros, G., Denfeld, B., and Pokrovsky, O. S.: Carbon  
802 emission from Western Siberian inland waters, *Nat. Commun.*, 12, 825, <https://doi.org/10.1038/s41467-021-21054-1>, 2021.

804 Kocic, J., Wallin, M. B., Chmiel, H. E., Denfeld, B. A., and Sobek, S.: Carbon dioxide evasion from  
805 headwater systems strongly contributes to the total export of carbon from a small boreal lake catchment,  
806 *J. Geophys. Res. Biogeosciences*, 120, 13–28, <https://doi.org/10.1002/2014JG002706>, 2015.

807 Koprivnjak, J.-F., Dillon, P. J., and Molot, L. A.: Importance of CO<sub>2</sub> evasion from small boreal streams, *Glob.*  
808 *Biogeochem. Cycles*, 24, GB4003, <https://doi.org/10.1029/2009GB003723>, 2010.

809 Krickov, I. V., Lim, A. G., Manasypov, R. M., Loiko, S. V., Shirokova, L. S., Kirpotin, S. N., Karlsson, J.,  
810 and Pokrovsky, O. S.: Riverine particulate C and N generated at the permafrost thaw front: Case study  
811 of western Siberian rivers across a 1700 km latitudinal transect, *Biogeosciences*, 6867–6884,  
812 <https://doi.org/10.5194/bg-15-6867-2018>, 2018.

813 Krickov, I. V., Serikova, S., Pokrovsky, O. S., Vorobyev, S. N., Lim, A. G., Siewert, M. B., and Karlsson, J.:  
814 Sizable carbon emission from the floodplain of Ob River, *Ecol. Indic.*, 131, 108164,  
815 <https://doi.org/10.1016/j.ecolind.2021.108164>, 2021.

816 Lauerwald, R., Laruelle, G. G., Hartmann, J., Ciais, P., and Regnier, P. A. G.: Spatial patterns in CO<sub>2</sub> evasion  
817 from the global river network, *Glob. Biogeochem. Cycles*, 29, 534–554,  
818 <https://doi.org/10.1002/2014GB004941>, 2015.

819 Leith, F. I., Dinsmore, K. J., Wallin, M. B., Billett, M. F., Heal, K. V., Laudon, H., Öquist, M. G., and Bishop,  
820 K.: Carbon dioxide transport across the hillslope–riparian–stream continuum in a boreal headwater  
821 catchment, *Biogeosciences*, 12, 1881–1892, <https://doi.org/10.5194/bg-12-1881-2015>, 2015.

822 Leng, P., Li, Z., Zhang, Q., Li, F., and Koschorreck, M.: Fluvial CO<sub>2</sub> and CH<sub>4</sub> in a lowland agriculturally  
823 impacted river network: Importance of local and longitudinal controls, *Environ. Pollution* 303, Art No  
824 119125, <https://doi.org/10.1016/j.envpol.2022.119125>, 2022.

825 Li, M., Peng, C., Zhang, K., Xu, L., Wang, J., Yang, Y., Li, P., Liu, Z., and He, N.: Headwater stream  
826 ecosystem: an important source of greenhouse gases to the atmosphere, *Water Res.*, 190, 116738,  
827 <https://doi.org/10.1016/j.watres.2020.116738>, 2021.

828 Liu S., Kuhn, C., Amatulli, G., Aho, K., Butman, D.E., Allen, G.H., Lin, P., Pan, M., Yamazaki, D.,  
829 Brinkerhoff, C., Gleason, C., Xia, X., and Raymond, P.A.: The importance of hydrology in routing  
830 terrestrial carbon to the atmosphere via global streams and rivers, *PNAS* 119 No. 11, e2106322119;  
831 <https://doi.org/10.1073/pnas.2106322119>, 2022.

832 Lobbes, J. M., Fitznar, H. P., and Kattner, G.: Biogeochemical characteristics of dissolved and particulate  
833 organic matter in Russian rivers entering the Arctic Ocean, *Geochim. Cosmochim. Acta*, 64, 2973–  
834 2983, [https://doi.org/10.1016/S0016-7037\(00\)00409-9](https://doi.org/10.1016/S0016-7037(00)00409-9), 2000.

835 Lorke A., Bodmer, P., Noss, C., Alshboul, Z., Koschorreck, M., Somlai-Haase, C., Bastviken, D., Flury, S.,  
836 McGinnis, D.F., Maeck, A., Müller, D., and Premke, K.: Technical note: drifting versus anchored  
837 flux chambers for measuring greenhouse gas emissions from running waters, *Biogeosciences*, 12,  
838 7013–7024, <https://doi.org/10.5194/bg-12-7013-2015>, 2015.

- 839 Lundin, E. J., Giesler, R., Persson, A., Thompson, M. S., and Karlsson, J.: Integrating carbon emissions from  
840 lakes and streams in a subarctic catchment, *J. Geophys. Res. Biogeosciences*, 118, 1200–1207,  
841 <https://doi.org/10.1002/jgrg.20092>, 2013.
- 842 Lynch, L. M., Sutfin, N. A., Feghel, T. S., Boot, C. M., Covino, T. P., and Wallenstein, M. D.: River channel  
843 connectivity shifts metabolite composition and dissolved organic matter chemistry, *Nat. Commun.*, 10,  
844 459, <https://doi.org/10.1038/s41467-019-08406-8>, 2019.
- 845 Marie, D., Partensky, F., Vaulot, D., and Brussaard, C.: Enumeration of Phytoplankton, Bacteria, and Viruses  
846 in Marine Samples, *Curr. Protoc. Cytom.*, 10, 11111–111115,  
847 <https://doi.org/10.1002/0471142956.cy1111s10>, 1999.
- 848 Pangala, S., Enrich-Prast, A., Basso, L., Peixoto, R. B., Bastviken, D., Hornibrook, E. R. C., Gatti, L. V.,  
849 Ribeiro, H., et al.: Large emissions from floodplain trees close the Amazon methane budget, *Nature*  
850 552, 230–234, <https://doi.org/10.1038/nature24639>, 2017.
- 851 Pekel, J.-F., Cottam, A., Gorelick, N., and Belward, A. S.: High-resolution mapping of global surface water  
852 and its long-term changes, *Nature*, 540, 418–422, <https://doi.org/10.1038/nature20584>, 2016.
- 853 Pokrovsky, O. S., Manasypov, R. M., Loiko, S., Shirokova, L. S., Krickov, I. A., Pokrovsky, B. G.,  
854 Kolesnichenko, L. G., Kopysov, S. G., Zemtsov, V. A., Kulizhsky, S. P., Vorobyev, S. N., and Kirpotin,  
855 S. N.: Permafrost coverage, watershed area and season control of dissolved carbon and major elements  
856 in western Siberian rivers, *Biogeosciences*, 12, 6301–6320, <https://doi.org/10.5194/bg-12-6301-2015>,  
857 2015.
- 858 Pokrovsky, O. S., Manasypov, R. M., Kopysov, S. G., Krickov, I. V., Shirokova, L. S., Loiko, S. V., Lim, A.  
859 G., Kolesnichenko, L. G., Vorobyev, S. N., and Kirpotin, S. N.: Impact of permafrost thaw and climate  
860 warming on riverine export fluxes of carbon, nutrients and metals in Western Siberia, *Water (MDPI)*,  
861 12, 1817, <https://doi.org/10.3390/w12061817>, 2020.
- 862 Pokrovsky, O. S., Manasypov, R. M., Chupakov, A. V., and Kopysov, S.: Element transport in the Taz River,  
863 western Siberia, *Chemical Geology*, 614, Art No 121180  
864 <https://doi.org/10.1016/j.chemgeo.2022.121180.2022>.
- 865 Ran, L., Lu, X. X., Richey, J. E., Sun, H., Han, J., Yu, R., Liao, S., and Yi, Q.: Long-term spatial and temporal  
866 variation of CO<sub>2</sub> partial pressure in the Yellow River, China, *Biogeosciences*, 12, 921–932,  
867 <https://doi.org/10.5194/bg-12-921-2015>, 2015.
- 868 Ran, L., Lu, X. X., and Liu, S.: Dynamics of riverine CO<sub>2</sub> in the Yangtze River fluvial network and their  
869 implications for carbon evasion, *Biogeosciences*, 14, 2183–2198, [https://doi.org/10.5194/bg-14-2183-](https://doi.org/10.5194/bg-14-2183-2017)  
870 2017, 2017.
- 871 Raymond, P. A., McClelland, J. W., Holmes, R. M., Zhulidov, A. V., Mull, K., Peterson, B. J., Striegl, R. G.,  
872 Aiken, G. R., and Gurtovaya, T. Y.: Flux and age of dissolved organic carbon exported to the Arctic  
873 Ocean: A carbon isotopic study of the five largest arctic rivers, *Glob. Biogeochem. Cycles*, 21, GB4011,  
874 <https://doi.org/10.1029/2007GB002934>, 2007.
- 875 Raymond, P. A., Zappa, C.J., Butman, D., Bott, T.L., Potter, J., Mulholland, P., Laursen, A. E., McDowell,  
876 W. H., and Newbold, D.: Scaling the gas transfer velocity and hydraulic geometry in streams and small  
877 rivers. *Limnology and Oceanography: Fluids and Environments*, 2(1), 41–53.  
878 <https://doi.org/10.1215/21573689-1597669>, 2012.
- 879 Raymond, P. A., Hartmann, J., Lauerwald, R., Sobek, S., McDonald, C., Hoover, M., Butman, D., Striegl,  
880 R., Mayorga, E., Humborg, C., Kortelainen, P., Dürr, H., Meybeck, M., Ciais, P., and Guth, P.: Global  
881 carbon dioxide emissions from inland waters, *Nature*, 503, 355–359,  
882 <https://doi.org/10.1038/nature12760>, 2013.
- 883 Rehder, Z., Zaplavnova, A., and Kutzbach, L.: Identifying drivers behind spatial variability of methane  
884 concentrations in East Siberian ponds. *Front. Earth Sci.* 9, Art No 617662, doi:  
885 [10.3389/feart.2021.617662](https://doi.org/10.3389/feart.2021.617662), 2021.
- 886 Rocher-Ros, G., Sponseller, R. A., Lidberg, W., Mörth, C.-M., and Giesler, R.: Landscape process domains  
887 drive patterns of CO<sub>2</sub> evasion from river networks, *Limnol. Oceanogr. Lett.*, 4, 87–95,  
888 <https://doi.org/10.1002/lol2.10108>, 2019.
- 889 Santoro, M., Beer, C., Cartus, O., Schullius, C., Shvidenko, A., McCallum, I., Wegmüller, U., and  
890 Wiesmann, A.: The BIOMASAR algorithm: An approach for retrieval of forest growing stock volume

- 891 using stacks of multi-temporal SAR data, in: Proceedings of ESA Living Planet Symposium, Bergen,  
892 Norway, 28 June – 2 July, 2010.
- 893 Schneider, C. L., Herrera, M., Raisle, M. L., Suarez, E., and Riveros-Iregui, D. A.: Carbon Dioxide (CO<sub>2</sub>)  
894 Fluxes from terrestrial and aquatic environments in a high altitude tropical catchment. *J Geophys.*  
895 *Res. Biogeosciences* 125, e2020JG005844. <https://doi.org/10.1029/2020JG005844>, 2020.
- 896 Semiletov, I. P., Pipko, I. I., Shakhova, N. E., Dudarev, O. V., Pugach, S. P., Charkin, A. N., McRoy, C. P.,  
897 Kosmach, D., and Gustafsson, Ö.: Carbon transport by the Lena River from its headwaters to the Arctic  
898 Ocean, with emphasis on fluvial input of terrestrial particulate organic carbon vs. carbon transport by  
899 coastal erosion, *Biogeosciences*, 8, 2407–2426, <https://doi.org/10.5194/bg-8-2407-2011>, 2011.
- 900 Serikova, S., Pokrovsky, O. S., Ala-Aho, P., Kazantsev, V., Kirpotin, S. N., Kopysov, S. G., Krickov, I. V.,  
901 Laudon, H., Manasypov, R. M., Shirokova, L. S., Soulsby, C., Tetzlaff, D., and Karlsson, J.: High  
902 riverine CO<sub>2</sub> emissions at the permafrost boundary of Western Siberia, *Nat. Geosci.*, 11, 825–829,  
903 <https://doi.org/10.1038/s41561-018-0218-1>, 2018.
- 904 Serikova, S., Pokrovsky, O. S., Laudon, H., Krickov, I. V., Lim, A. G., Manasypov, R. M., and Karlsson, J.:  
905 High carbon emissions from thermokarst lakes of Western Siberia, *Nat. Commun.*, 10,  
906 <https://doi.org/10.1038/s41467-019-09592-1>, 2019.
- 907 **Spawn, S. A., Dunn, S. T., Fiske, G. E., Natali, S. M., Schade, J. D., and Zimov, N. S.: Summer methane**  
908 **ebullition from a headwater catchment in Northeastern Siberia, *Inland Waters*, 5(3), 224-230, DOI:**  
909 **[10.5268/IW-5.3.845](https://doi.org/10.5268/IW-5.3.845), 2015.**
- 910 Stackpoole, S. M., Butman, D. E., Clow, D. W., Verdin, K. L., Gaglioti, B. V., Genet, H., and Striegl, R. G.:  
911 Inland waters and their role in the carbon cycle of Alaska, *Ecol. Appl.*, 27, 1403–1420,  
912 <https://doi.org/10.1002/eap.1552>, 2017.
- 913 **Stanley, E. H., Casson, N. J., Christel, S. T., Crawford, J. T., Loken, L. C., and Oliver, S.K.: The ecology of**  
914 **methane in streams and rivers: patterns, controls, and global significance, *Ecol. Monogr.* 86, 146–171,**  
915 **2016.**
- 916 Striegl, R. G., Dornblaser, M. M., McDonald, C. P., Rover, J. A., and Stets, E. G.: Carbon dioxide and  
917 methane emissions from the Yukon River system, *Glob. Biogeochem. Cycles*, 26, GB0E05,  
918 <https://doi.org/10.1029/2012GB004306>, 2012.
- 919 Teodoru, C. R., del Giorgio, P. A., Prairie, Y. T., and Camire, M.: Patterns in pCO<sub>2</sub> in boreal streams and  
920 rivers of northern Quebec, Canada, *Glob. Biogeochem. Cycles*, 23, GB2012,  
921 <https://doi.org/10.1029/2008GB003404>, 2009.
- 922 Tranvik, L., Cole, J. J., and Prairie, Y. T.: The study of carbon in inland waters-from isolated ecosystems to  
923 players in the global carbon cycle, *Limnol. Oceanogr. Lett.*, 3, 41–48,  
924 <https://doi.org/10.1002/lol2.10068>, 2018.
- 925 Vachon, D., Sponseller, R. A., and Karlsson, J.: Integrating carbon emission, accumulation and transport in  
926 inland waters to understand their role in the global carbon cycle, *Glob. Change Biol.*, 27, 719–727,  
927 <https://doi.org/10.1111/gcb.15448>, 2021.
- 928 **Villa, J. A., Ju, Y., Yazbeck, T., Waldo, S., Wrighton, K. C., and Bohrer, G.: Ebullition dominates methane**  
929 **fluxes from the water surface across different ecohydrological patches in a temperate freshwater marsh**  
930 **at the end of the growing season, *Sci. Total Environ.* 767, 144498, 2021.**
- 931 Vorobyev, S. N., Pokrovsky, O. S., Kolesnichenko, L. G., Manasypov, R. M., Shirokova, L. S., Karlsson, J.,  
932 and Kirpotin, S. N.: Biogeochemistry of dissolved carbon, major, and trace elements during spring flood  
933 periods on the Ob River, *Hydrol. Process.*, 33, 1579–1594, <https://doi.org/10.1002/hyp.13424>, 2019.
- 934 Vorobyev, S. N., Karlsson, J., Kolesnichenko, Y. Y., Korets, M. A., and Pokrovsky, O. S.: Fluvial carbon  
935 dioxide emission from the Lena River basin during the spring flood, *Biogeosciences*, 18, 4919–4936,  
936 <https://doi.org/10.5194/bg-18-4919-2021>, 2021.
- 937 Wallin, M. B., Öquist, M. G., Buffam, I., Billett, M. F., Nisell, J., and Bishop, K. H.: Spatiotemporal  
938 variability of the gas transfer coefficient (KCO<sub>2</sub>) in boreal streams: Implications for large scale  
939 estimates of CO<sub>2</sub> evasion, *Glob. Biogeochem. Cycles*, 25, GB3025,  
940 <https://doi.org/10.1029/2010GB003975>, 2011.
- 941 Wallin, M. B., Grabs, T., Buffam, I., Laudon, H., Ågren, A., Öquist, M. G., and Bishop, K.: Evasion of CO<sub>2</sub>  
942 from streams – The dominant component of the carbon export through the aquatic conduit in a boreal  
943 landscape, *Glob. Change Biol.*, 19, 785–797, <https://doi.org/10.1111/gcb.12083>, 2013.

944 Wallin, M. B., Campeau, A., Audet, J., Bastviken, D., Bishop, K., Kokic, J., Laudon, H., Lundin, E., Löfgren,  
945 S., Natchimuthu, S., Sobek, S., Teutschbein, C., Weyhenmeyer, G. A., and Grabs, T.: Carbon dioxide  
946 and methane emissions of Swedish low-order streams—a national estimate and lessons learnt from  
947 more than a decade of observations, *Limnol. Oceanogr. Lett.*, 3, 156–167,  
948 <https://doi.org/10.1002/lol2.10061>, 2018.

949 Wild, B., Andersson, A., Bröder, L., Vonk, J., Hugelius, G., McClelland, J. W., Song, W., Raymond, P. A.,  
950 and Gustafsson, Ö.: Rivers across the Siberian Arctic unearth the patterns of carbon release from  
951 thawing permafrost, *PNAS*, 116, 10280–10285, <https://doi.org/10.1073/pnas.1811797116>, 2019.

952 Winterdahl, M., Wallin, M. B., Karlsen, R. H., Laudon, H., Öquist, M., and Lyon, S. W.: Decoupling of  
953 carbon dioxide and dissolved organic carbon in boreal headwater streams, *J. Geophys. Res.*  
954 *Biogeosciences*, 121, 2630–2651, <https://doi.org/10.1002/2016JG003420>, 2016.

955 Yamamoto, S., Alcauskas, J. B., and Crozier, T. E.: Solubility of methane in distilled water and seawater. *J.*  
956 *Chem. Eng. Data*. 21, 78–80, 1976.

957 Zabelina, S. V., Shirokova, L. S., Klimov, S I., Chupakov, A. V., Lim, A. G., Polishchuk, Y. M., Polishchuk,  
958 V. M., Bogdanov, A. N., Muratov, I. N., Gueren, F., Karlsson, J., and Pokrovsky, O. S.: Seasonal and  
959 spatial variations of CO<sub>2</sub> and CH<sub>4</sub> concentrations and fluxes in surface waters of frozen peatlands (NE  
960 Europe): morphological and hydrochemical control, *Limnology Oceanography*, 66 (S1), S216-S230,  
961 doi: 10.1002/lno.11560, 2021.

962 Zolkos, S., Tank, S. E., Striegl, R. G., and Kokelj, S. V.: Thermokarst effects on carbon dioxide and methane  
963 fluxes in streams on the Peel Plateau (NWT, Canada), *J. Geophys. Res. Biogeosciences*, 124, 1781–  
964 1798, <https://doi.org/10.1029/2019JG005038>, 2019.

965

966

967

968

969

970

971

972

973

974

975

976

977

978

979

980

981

982

983

984

985

986  
987  
988  
989  
990  
991  
992  
993

**Table 1.** Measured hydrochemical and GHG exchange parameters in the Ket River main stem and tributaries (average  $\pm$  s.d.; (*n*) is number of measurements). The FCO<sub>2</sub> and K<sub>T</sub> are chamber-measured CO<sub>2</sub> flux and gas transfer velocity, respectively, whereas diffusive CH<sub>4</sub> flux (FCH<sub>4</sub>) was calculated using chamber-specific transfer coefficient.

Parameter	unit	Tributaries		Main stem	
		Flood ( <i>n</i> =26)	Base flow ( <i>n</i> =12)	Flood ( <i>n</i> =7)	Base flow ( <i>n</i> =6)
Water temperature	°C	9.48±2.25	14.9±1.24	9.06±1.59	16.5±0.54
pH		6.31±0.45	6.71±0.57	6.2±0.43	7.29±0.26
Dissolved O <sub>2</sub>	mg L <sup>-1</sup>	8.53±1.26	8.02±1.13	8.85±0.83	8.78±0.18
Specific Conductivity	µS cm <sup>-1</sup>	40.7±22.7	126.9±62.1	39±14.9	181±36.8
DIC	mg L <sup>-1</sup>	2.83±2.58	17.8±10.4	2.43±1.49	20.5±5.22
DOC	mg L <sup>-1</sup>	21.7±3.94	15.7±7.04	21.9±4.28	16.6±3.57
SUVA <sub>254</sub>	L mg C <sup>-1</sup> m <sup>-1</sup>	4.34±0.33	4.9±0.66	4.29±0.18	4.26±0.52
PON	mg L <sup>-1</sup>	0.08±0.06	0.64±0.27	0.1±0.07	0.96±0.22
POC	mg L <sup>-1</sup>	2.41±1.17	8±2.36	2.55±1.2	9.49±1.98
TBC	*10 <sup>5</sup> cells ml <sup>-1</sup>	5.89±3.26	8.69±3.21	5.95±2.83	4.94±2.15
K <sub>T</sub>	m d <sup>-1</sup>	0.53±0.38	1.21±0.52	0.77±0.55	1.22±0.37
FCO <sub>2</sub>	g C m <sup>-2</sup> d <sup>-1</sup>	1.3±0.76	2.63±2.15	1.35±1.08	1.16±0.5
pCO <sub>2</sub>	µatm	2880±680	4000±1500	2400±330	2520±980
FCH <sub>4</sub>	mmol C m <sup>-2</sup> d <sup>-1</sup>	0.39±0.95	1.38±1.21	0.06±0.05	0.95±0.88
CH <sub>4</sub>	µmol L <sup>-1</sup>	0.65±0.66	1.17±0.81	0.17±0.01	0.86±0.91

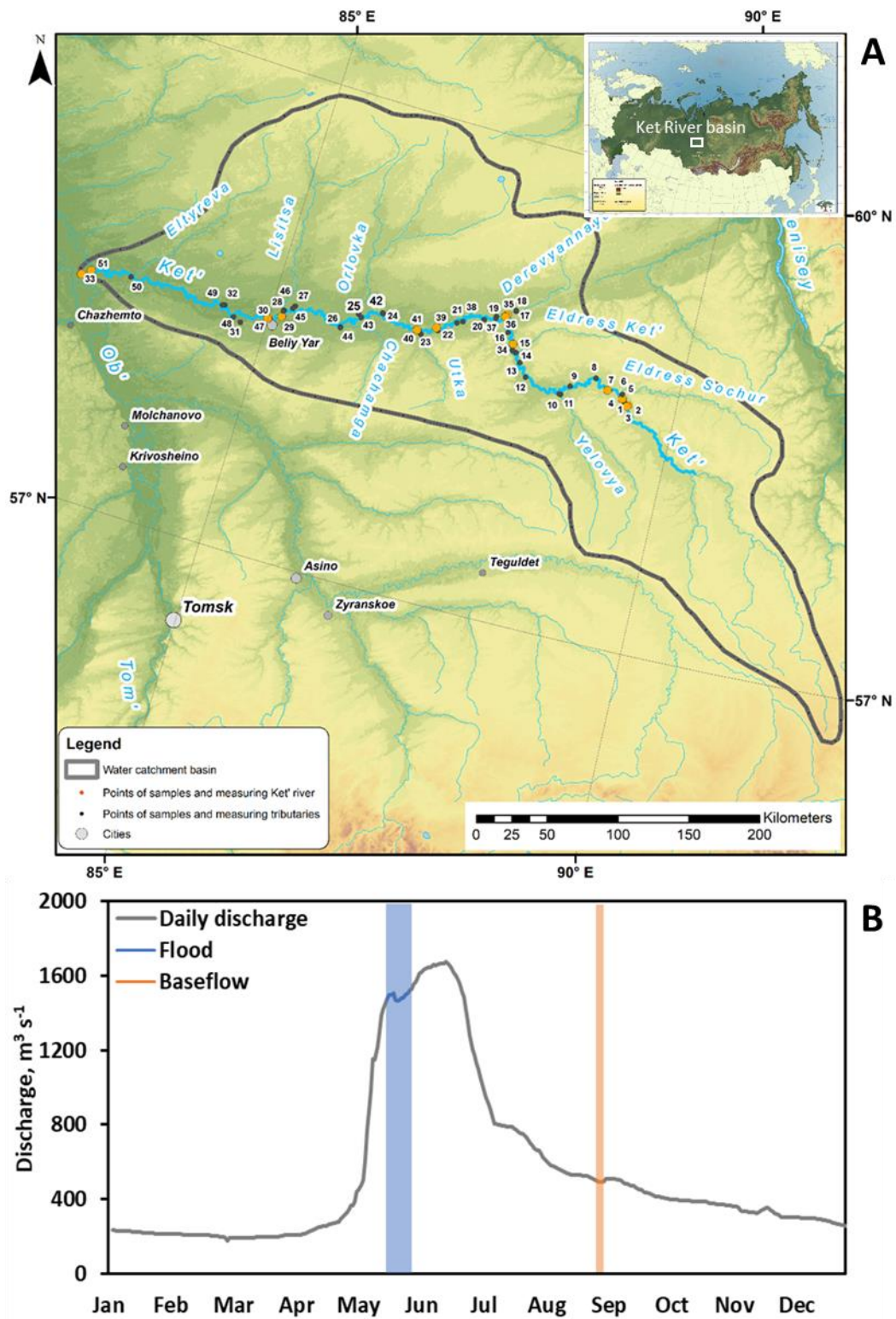
994  
995  
996  
997  
998  
999  
1000  
1001  
1002  
1003  
1004  
1005  
1006  
1007  
1008  
1009  
1010  
1011  
1012  
1013  
1014  
1015  
1016

1017  
 1018  
 1019  
 1020  
 1021  
 1022  
 1023  
 1024  
 1025  
 1026  
 1027

**Table 2.** Pearson correlation coefficients of measured FCO<sub>2</sub>, CO<sub>2</sub>, and CH<sub>4</sub> concentration with hydrochemical parameters of the water column (DOC, SUVA, particulate organic carbon and nitrogen, total bacterial cells) and landscape parameters of the tributaries and the main stem of the Ket River. Significant (p < 0.05) values are labeled by asterisk.

	all seasons			spring flood			summer baseflow		
	CH <sub>4</sub>	CO <sub>2</sub>	FCO <sub>2</sub>	CH <sub>4</sub>	CO <sub>2</sub>	FCO <sub>2</sub>	CH <sub>4</sub>	CO <sub>2</sub>	FCO <sub>2</sub>
<b>Hydrochemical parameters</b>									
pH	0.2	-0.1	-0.2	-0.1	0.1	-0.2	0.0	-0.6*	-0.6*
Dissolved O <sub>2</sub>	-0.1	-0.7*	-0.1	0.0	-0.8*	0.1	-0.2	-0.8*	-0.7*
Specific conductivity	0.3	0.0	0.1	-0.2	0.0	0.1	0.2	-0.3	-0.6*
DIC	0.3	0.0	0.0	-0.1	0.0	0.1	0.2	-0.4	-0.7*
DOC	-0.1	0.0	0.1	0.3	0.0	-0.1	-0.2	-0.1	0.2
SUVA <sub>254</sub>	0.1	0.2	0.3	0.4	-0.3	0.1	-0.2	0.5*	0.6*
PON	0.1	-0.1	0.2	-0.2	-0.4*	0.2	-0.4	-0.5*	-0.5
POC	0.1	-0.1	0.2	-0.2	-0.4*	0.1	-0.3	-0.3	0.1
TBC	0.2	0.2	0.1	0.3	-0.2	-0.1	0.0	0.5*	0.5*
<b>Climatic characteristics</b>									
MAAT	0.2	0.0	-0.5*	0.1	0.0	-0.4*	0.2	0.1	-0.5
MAP	0.0	0.3*	0.5*	0.1	0.0	0.3	0.1	0.6*	0.7*
<b>Land-cover characteristics</b>									
Watershed area	-0.3	-0.3*	0.2	-0.4	-0.5*	0.0	-0.2	-0.1	0.5
Dark Needleleaf Forest	0.1	0.0	-0.3	0.1	0.0	-0.3	0.2	-0.1	-0.2
Light Needleleaf Forest	0.3*	0.4*	0.2	0.4	0.2	0.0	0.4	0.7*	0.6*
Broadleaf Forest	-0.3	-0.4*	0.1	-0.5*	-0.4	0.1	-0.3	-0.6*	-0.2
Mixed Forest	0.0	-0.2	-0.3	0.1	-0.1	-0.3	-0.1	-0.4	-0.4
Peatlands and bogs	0.0	0.2	0.3	-0.1	0.0	0.2	0.1	0.2	0.4
Riparian Vegetation	-0.1	0.0	-0.1	-0.2	0.1	0.0	-0.2	-0.2	-0.5
Grassland	0.1	-0.1	0.0	-0.1	-0.2	0.1	0.3	0.0	-0.5
Recent Burns	-0.1	-0.1	0.2	-0.1	-0.2	0.1	-0.3	0.1	0.4
Water Bodies	-0.2	-0.1	0.3	-0.3	-0.3	0.2	-0.2	-0.1	0.3

1028  
 1029  
 1030  
 1031  
 1032  
 1033  
 1034



1035

1036

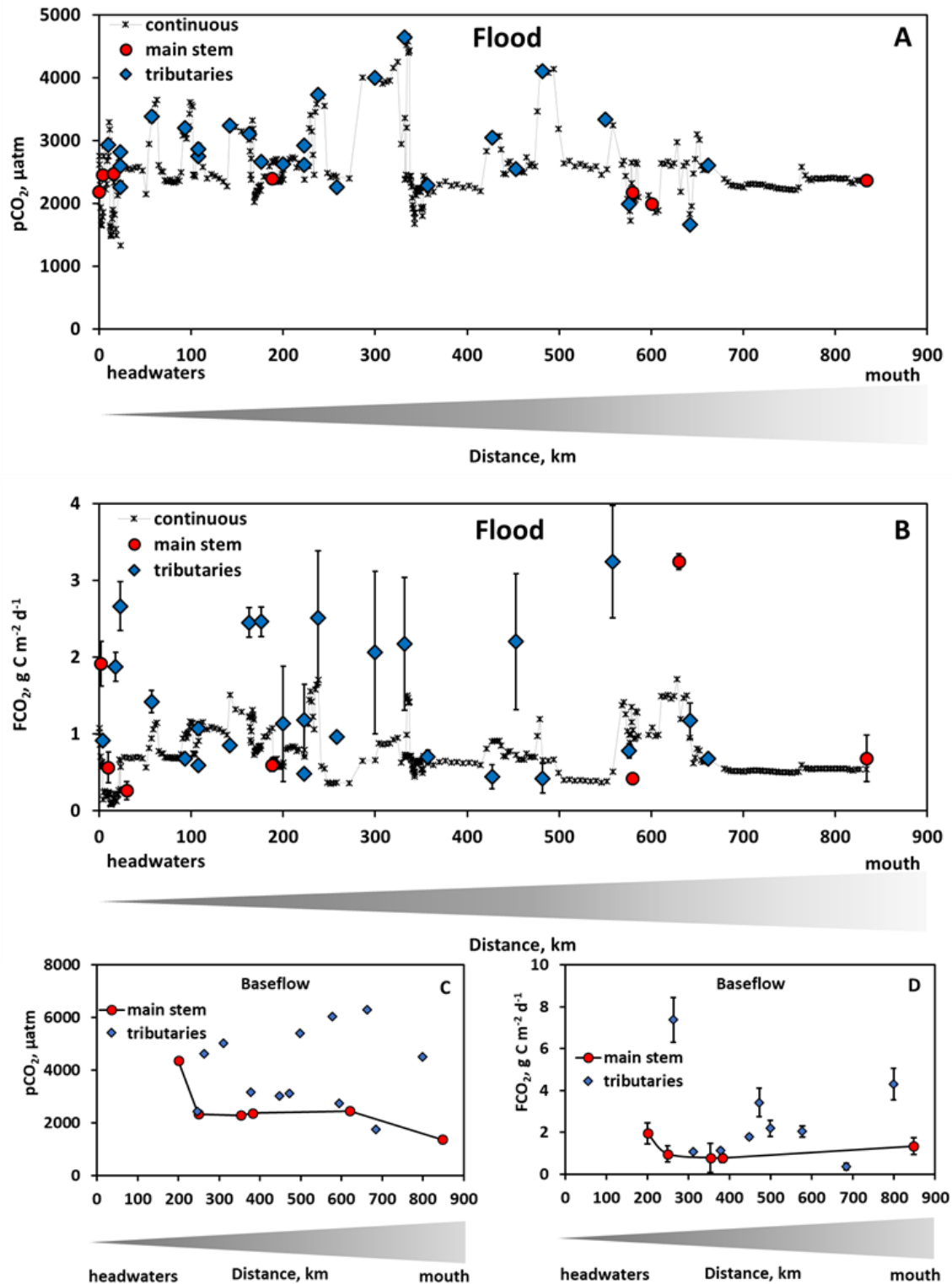
1037 **Fig. 1. A:** Map of the studied Ket River watershed with continuous pCO<sub>2</sub> measurements in the main stem.

1038 **B:** Daily discharge (Q) at the gauging station of the Ket mouth, Rodionovka, in 2019. Highlighted in blue

1039 and orange are two sampling campaigns of this study, spring flood and summer-autumn baseflow.

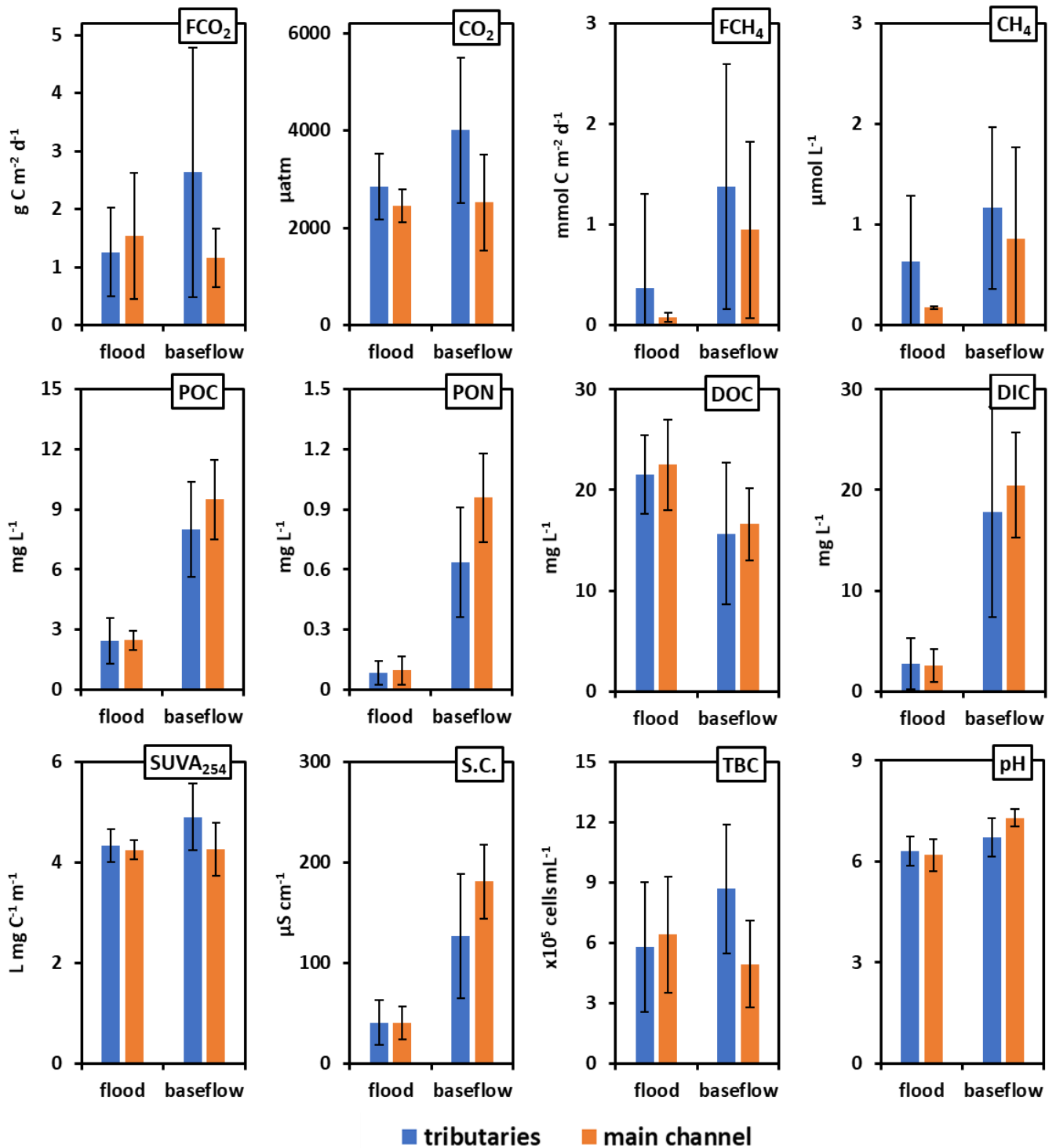
1040

1041



1042

1043 **Figure 2.** The measured pCO<sub>2</sub> (A, C) and CO<sub>2</sub> fluxes (B, D) during spring flood (A, B) and summer  
 1044 baseflow (C, D) of the Ket River main stem and tributaries (over the 830 km distance, from the headwaters to  
 1045 the mouth (left to right)). The symbols represent discrete in situ pCO<sub>2</sub> (Vaissala) and FCO<sub>2</sub> (floating  
 1046 chambers) measurements of the main stem (red circles) and tributaries (blue diamonds). Continuous in-situ  
 1047 pCO<sub>2</sub> measurements and calculated FCO<sub>2</sub> are available only for the main stem in spring (black crosses). For  
 1048 the latter, we used an average value of **measured** gas transfer velocity ( $K_T$ ) between two chamber sites  
 1049 (separated by a distance of 50 to 100 km) to calculate the FCO<sub>2</sub> from in-situ measured pCO<sub>2</sub> in the river  
 1050 section between these two sites. Note that during summer baseflow, the water level did not allow reaching  
 1051 the headwaters of the Ket River (first 0-200 km on the river course).



1052

1053

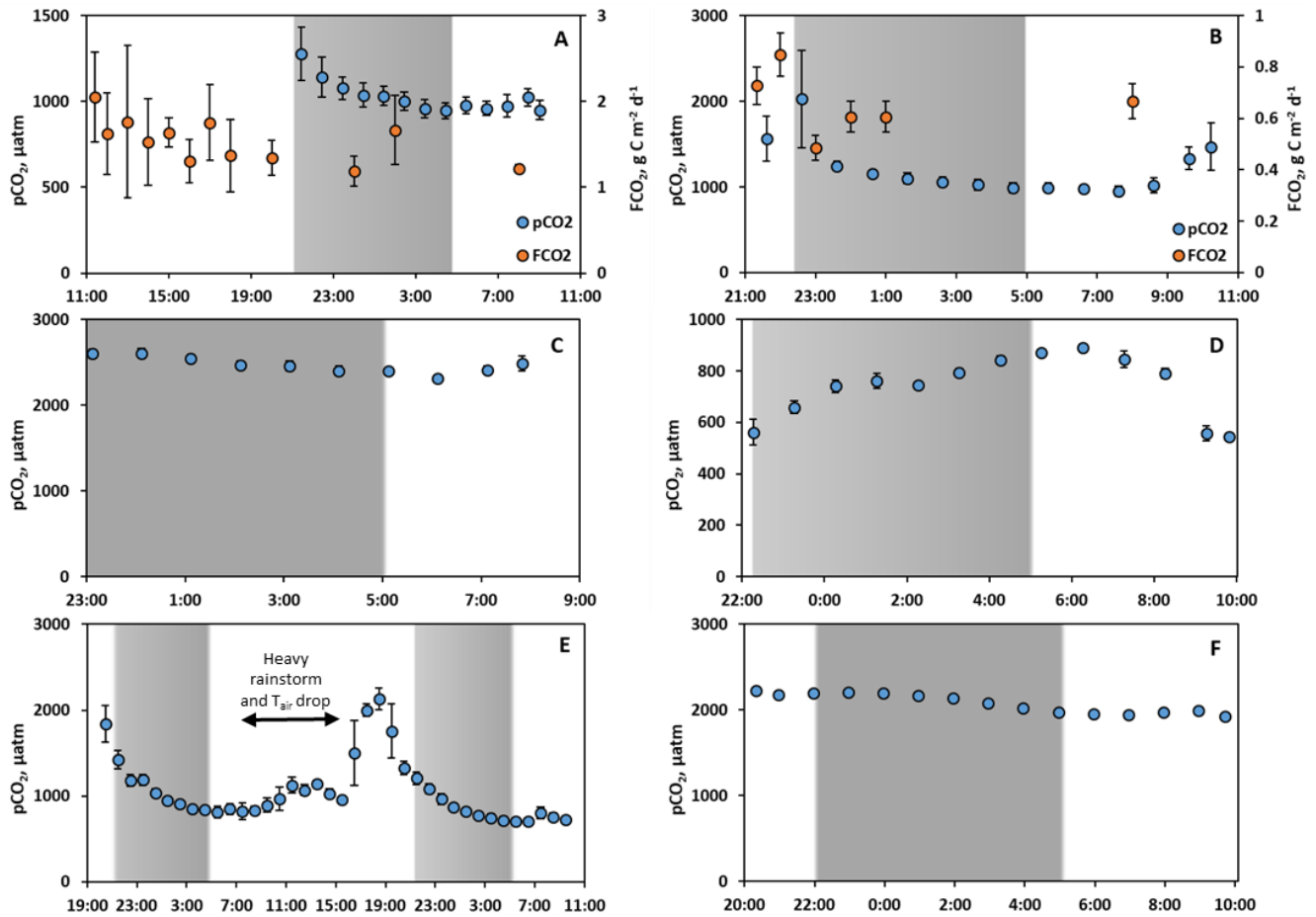
1054

1055 **Figure 3.** Mean ( $\pm$  s.d.) GHG concentration and chamber-measured fluxes ( $FCO_2$ ), hydrochemical  
 1056 parameters, particulate organic carbon and nitrogen (POC and PON, respectively) and total bacteria count  
 1057 (TBC), in the main channel (orange column) and the tributaries (blue column) of the Ket River in spring  
 1058 flood and summer (early fall) baseflow.

1059

1060

1061



1063

1064

1065

1066

1067

**Figure 4.** Continuous pCO<sub>2</sub> concentration (A-F, blue circles) and chamber-based fluxes (A, B) measured during spring flood period in tributaries (A Sochur No 3, B Lopatka No 8, C Derevyannaya No 12, D Ob river entrance, E Segondenka No 26) and in the Ket River main stem (middle course) near Stepanovka village (F) including night time measurements (shaded area). The measurement frequency was one per hour. Variations of water temperature were within the range of 0.3 to 0.6 °C and did not exhibit significant correlations with pCO<sub>2</sub> and FCO<sub>2</sub>. Note that, for the small river Segondenka ( $S_{\text{watershed}} = 472 \text{ km}^2$ ), where the CO<sub>2</sub> peak was observed at 7 pm (E), there was quite heavy rainfall between 7 am and 3 pm.

1075

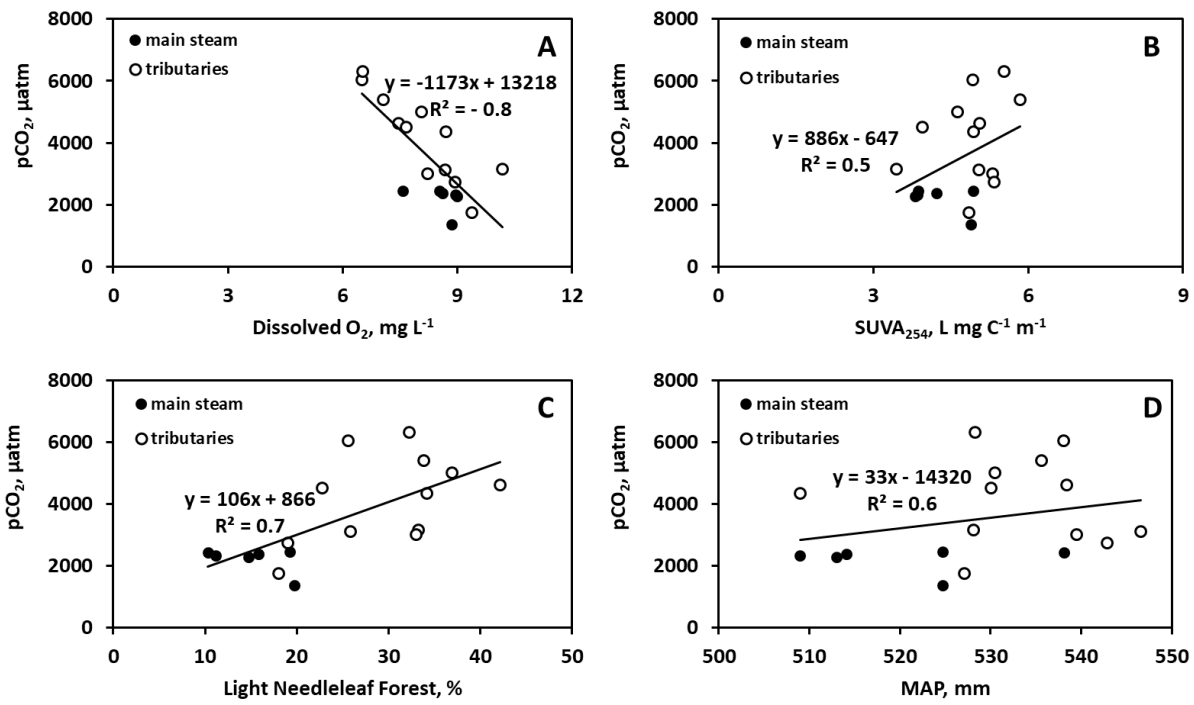
1076

1077

1078

1079

1080  
1081  
1082  
1083



1084  
1085  
1086  
1087  
1088  
1089  
1090  
1091  
1092  
1093  
1094  
1095  
1096  
1097

**Figure 5.** Significant ( $p < 0.05$ ) control of dissolved oxygen (A),  $\text{SUVA}_{254}$  (B), light needleleaf forest (C), and mean annual precipitation (D) on  $\text{CO}_2$  concentration in the Ket River and tributaries during summer baseflow.